4

Theoretical Modeling of Cyclically Loaded, Biodegradable Cylinders

J. S. Soares,

Department of Mechanical Engineering
Texas A&M University
College Station, TX 77843, USA

J. E. Moore, Jr.,

Department of Biomedical Engineering
Texas A&M University
College Station, TX 77843, USA

AND

K. R. Rajagopal

Department of Mechanical Engineering and
Department of Biomedical Engineering
Texas A&M University
College Station, TX 77843, USA

Abstract. The adaptation of fully biodegradable stents, thought to be the next revolution in minimally invasive cardiovascular interventions, is

supported by recent findings in cardiovascular medicine concerning human coronaries and the likelihood of their deployment has been made possible by advances in polymer engineering. The main potential advantages of biodegradable polymeric stents are: (1) the stent can degrade and transfer the load to the healing artery wall which allows favorable remodeling, and (2) the size of the drug reservoir is dramatically increased. The in-stent restenotic response usually happens within the first six months, thus a fully biodegradable stent can fulfill the mission of restoring flow while mitigating the probability of long-term complications. However, it is a key concern that the stent not degrade away too soon, or develop structural instabilities due to faster degradation in key portions of the stent. We present here a preliminary model of the mechanics of a loaded, biodegradable cylindrical structure. The eventual goal of this research is to provide a means of predicting the structural stability of biodegradable stents.

As a first step towards a fully nonlinear model, biodegradable polymers are modeled as a class of linearized materials. An inhomogeneous field that reflects the degradation, which we henceforth refer to as degradation, and a partial differential equation governing the degradation are defined. They express the local degradation of the material and its relationship to the strain field. The impact of degradation on the material is accomplished by introducing a time-dependent Young's modulus function that is influenced by the degradation field. In the absence of degradation, one recovers the classical linearized elastic model. The rate of increase of degradation was assumed to be dependent on time and linearized strain with the following characteristics: (1) a material degrades faster when it is exposed to higher strains, and (2) a material that is strained for a longer period of time degrades more rapidly than a material that has been strained by the same amount for a shorter period of time.

The initial boundary value problem considered is that of an infinitely long, isotropic, nearly incompressible, homogeneous, and strain-degradable cylindrical annulus subjected to radial stresses at its boundaries. A semi-inverse method assuming a specific form of the displacement field was employed and the problem reduced to two coupled nonlinear partial differential equations for a single spatial coordinate and time. These equations were solved simultaneously for the displacement and degradation fields using a time marching finite element formulation with a set of nonlinear iterations for each time step.

The main features that were observed were: (1) strain-induced degradation showed acceptable phenomenological characteristics (i.e. progressive failure of the material and parametric coherence with the defined constants); (2) an inhomogeneous deformation leads to inhomogeneous degradation and therefore in an initially homogeneous body the properties vary with the current location of the particles; and (3) the linearized model,

in virtue of degradation, exhibits creep, stress relaxation, and hysteresis, but this is markedly different from the similar phenomena exhibited by viscoelastic materials.

4.1 Cardiovascular Stents

Since the introduction of angioplasty by Dotter in the 1960s [DOa], catheter-based technologies have improved health care for atherosclerosis. Well over a million balloon dilatations were performed by the early 1990s and as of today more than 600,000 a year are carried out in coronary arteries alone [LIf]. Yet, after more than 20 years of clinical experience and many catheter designs, angioplasty was far from being perfect and the incidence of restenosis remained unchanged. Many studies reported acute complications in 3% to 5% of the patients and restenosis rates at 3 to 6 months between 25 and 50% [GLb, MUa]. Restenosis seemed to be largely independent of the technique, device, or the clinician's skill [ROc, DOb, SAb]. The pathophysiology of restenosis is complex and incompletely understood. Early events in restenosis are thought to consist of immediate elastic recoil, platelet deposition, and thrombus formation, followed by smooth muscle cell proliferation and matrix formation [LIc, CUa, MIc].

Percutaneous implantation of metallic stents in the coronary vessels was first performed in humans in 1987 by Sigwart et al. [SIb]. During the late 1990s, stents revolutionized the field of interventional cardiology and stent implantation has become the new standard angioplasty procedure [ALa]. The major design concept behind cardiovascular stents was to prevent post-traumatic vasospasm [SIb]. Besides keeping the artery patent immediately after intervention, a stent also tackles injured flaps of the lumen preventing downstream embolic complications [PAa, SCc]. Although the concept seemed to be flawless and a significant reduction of the incidence of restenosis was promptly reported [SEa, FIb], all cardiovascular stents have two distinct and significant modes of chronic failure. Immediately after deployment acute thrombosis can occur due to the thrombogenic aspect of the stent promoting a foreign body response, but it can be promptly treated with anticoagulant drug therapy [SCb]. Also the most critical failure mode is in-stent restenosis which still occurs at intolerable rates. Despite the success and growth of stent implantation procedures, there are patients in whom in-stent restenosis is a chronic and recurrent problem [MIb]. The mechanism of in-stent restenosis can be obviously related with restenosis after angioplasty as well as with atherosclerosis and has been shown to be neointimal proliferation in response to injury [SCf] and not chronic stent recoil [SCg].

The reaction of the artery to a stent is a multistage process [EDa]. First, the exposure of the subendothelium and the stent material to the blood stream activates platelets and leads to thrombus formation. This process is initiated immediately after deployment and the extent to which the thrombus deposition occurs is highly correlated not only with the surface characteristics of the stent but also with its design. Areas of flow stagnation, which depend heavily on strut design, influence the degree of platelet adhesion [ROa]. The second stage is inflammation. Stenting overstretches and may even rupture the internal elastic membrane inducing leukocyte adhesion and consequent inflammatory reaction [ROb]. The peak of this process occurs approximately one week after deployment. Deposits of surface adherent and tissue infiltrating monocytes can be seen around stent struts, demonstrating the degree to which the struts are injuring the wall. These monocytes release cytokines, mitogens, and tissue growth factors that further increase neointimal formation [FAa]. The third stage is the proliferation of vascular smooth muscle cells in the media and neointima. This process can be thought as the short-term response to the change in hemodynamics and the wall's response after stent placement [WEc, WEd]. Cellular proliferation provides additional tissue to shore up stress concentrations due to stent deployment [MOa]. The final stage of arterial adaptation is remodeling. One can think of this phase as the artery's attempt to reach a new homeostatic state in the presence of persistent injury and change in the normal environment caused by the stent [GLa].

Systemically administered pharmaceutical agents, besides pre- and post interventional anticoagulant therapies, fail to prevent restenosis because the tolerated dose for such agents is too low to achieve a sufficient drug concentration at the targeted site [LIe]. The problem of in-stent restenosis is currently being addressed by coating stents with polymers in which drugs can be impregnated and locally delivered. Polymers provide a stable medium into which drugs can be either uniformly distributed or surface layered and then locally released over a specific and controlled period of time, usually between weeks to months [WHa]. The first reports of local drug delivery in the cardiovascular system date back only to the mid 1990s with forskolin [LAb] and heparin [AHa]. Success with anti-inflammatory dexamethasome was reported by Lincoff et al. in 1997 [LId]. Suppression of restenotic proliferative stimuli was achieved by Yamawaki et al. in 1998 [YAa]. Successful gene transfer and expression following implantation of polymer stents impregnated with a recombinant adenovirus gene was demonstrated by Ye et al. in 1998 [YEa]. The objective of the pharmacological agents used in drug eluting stents is to address a particular stage of the restenotic cascade: heparin is loaded into stents in order to inhibit the thrombus formation [AHa] and inflammation is prevented with dexamethasone [LId]. The most effective drugs are antimitotic agents that prevent the proliferation stage. As of now, the two most effective and well-studied

pharmacological agents for this outcome are Paclitaxel and Sirolimus. Paclitaxel inhibits microtubule depolymerization, and thereby has potent effects in cell division and migration [AXa]. Sirolimus is a macrolide antibiotic with potent antiproliferative effects on vascular smooth muscle cells preventing the initiation of DNA synthesis [MAa, GAa].

The use of drug eluting stents generally improves the success of coronary interventions. In fact, drug eluting stents are now considered general practice [SAa]. Several randomized studies have been carried out and are still ongoing with the objective to evaluate the efficacy of the drugs with regard to their release kinetics, effective dosage, and the benefit of such a particular pharmacological approach [GRc]. Two major randomized trials have been carried out: the RAVEL randomized trial with several followup SIRIUS studies, with Sirolimus eluting stents, showed promising zero restenosis at six months in 238 patients [MOb, MOc], and good results all across the most common subsets of patients and lesion types [MOc, SCe, ARa]; and the TAXUS series of randomized trials, a Paclitaxel eluting stent, also exhibited good restenosis results [GRd, TAe, STb]. As of today, only two polymer-coated drug eluting stents (Cypher^{TM} Sirolimus eluting stent from Cordis, Johnson & Johnson, Miami Lake, FL, USA, and the Taxus^{TM} Paclitaxel eluting stent, Boston Scientific, Natick, MA, USA, introduced in February 2003) are commercially available. Several registries are in effect in several European countries [LEa, ZAa, ONa] (less data on the Paclitaxel eluting stent are available: Cypher^{TM} was introduced in 2002, Taxus^{TM} in February 2003) and show similar results with regard to the two stents and good "real world" success rates ($\approx 1\%$ stent thrombosis, $\approx 10\%$ angiographic restenosis, $\approx 7\%$ target lesion revascularization) [KAa].

Obviously, some problems have been reported for drug eluting stents. Delayed stent thrombosis due to incomplete endothelialization of the stent struts is still a problem with stents, drug eluting or not [JEa]. The "catch-up" effect after the complete elution of the drug raised some concerns [VIa], and the lack of long-term followup studies still haunts this technology. Another limitation is the emphasis given to drug eluting stent implantations on coronaries; only a limited amount of data exists on their application in peripheral arteries. In the SCIROCCO trials, Sirolimus eluting stents deployed in long lesions in peripheral arteries, showed promising short-term results (6% restenosis at 6 months) but no difference relative to bare metal stents after 18 months [DUa, DUb].

4.2 Biodegradable Stents

There are some theoretical concerns with metallic stents: (1) most metals are electropositively charged, resulting in high thombogenicity [DEc],

(2) in addition, metal stents remain in the body indefinitely and may interfere with future clinical procedures [AGb]; and (3) due to their microstructural properties, metals are not feasible materials to act as loadable drug carriers. All these problems have encouraged significant efforts in the development of new stent materials, either used in coatings [VAe] or in stents completely made of polymeric materials [MUc]. Polymers can also act as optimal carriers for the controlled release of drugs [PEa].

One possible objective in coating a metal stent is to diminish its thrombogenic properties [DEb]. Experience with Nylon^{TM}, silicone, polyurethane, and other materials have been reported in the literature since the beginning of the 1990s [BEc]. Either naturally occurring polymers (fibrin [HOa]) or pharmacological agents (heparin [SEb], dexamethasone [LId], and others [BAa]) relevant to the local biochemistry of the lesion were tested in vivo as coatings. The use of polymers in stent coatings requires less mechanical requisites from the polymer by itself and shifts the attention mostly to biocompatibility and to manufacturability. Still, poor adherence of the coating to the metal, possible delamination with strain, or damage during implantation are problems that may occur [SIc].

Interest in polymeric stents started in the 1990s. Significant progress has been achieved in increasing the level of biocompatibility of polymers tailoring surface characteristics and mechanical strength through advancements in polymerization procedures and processing techniques [PEa]. In 1992, Murphy et al. demonstrated the technical feasibility of polyethylene terephthalate stents but obtained poor results in porcine coronaries, particularly an intense proliferative neointimal response that resulted in complete vessel occlusion [MUb]. On the other hand, around the same time, van der Giessen et al. showed acceptable results with stents made of the same material deployed in the same animal model [VAd]. The extent of neointimal proliferation was similar to that observed after the placement of metal stents (obviously, compared with the standards of that time), despite the presence of a more pronounced inflammatory reaction [VAc]. Later in 1996, van der Giessen et al. investigated the biocompatibility of an array of both biodegradable and nonbiodegradable polymers (polyglycolic acid/polylactic acid, polycaprolactone, polyhydroxybutyrate valerate, polyorthoester, and polyethyleneoxide/polybutylene terephthalate) for stent coating and found a marked inflammatory reaction with subsequent neointimal thickening in all of them [VAb]. The experimental procedure used was completely inappropriate, in that the stents were not sterilized before implantation [FIa]. The biocompatibility of these polymers has been proven in other in vitro and in vivo tests [DEb, DEa].

Because of this general disagreement on the biocompatibility of polymers, the idea of either biodegradable or biostable polymers, which had considerable appeal during the early 1990s, was set aside. The interest peaked in

1994 with Zidar's chapter included in the second edition of the *Textbook of Interventional Cardiology* dedicated in full to the topic of biodegradable stents [ZIa]. Later in 2000, Tamai et al. should be credited with rekindling the resurgence of employing fully biodegradable stents. They provided the first report on the immediate and six-month results after implantation of biodegradable poly-L-lactic acid stents in humans. With their good initial results [TAb] (obviously, compared with the standards before the drug eluting stents era), the motivation for fully biodegradable stents was flourishing once again [FAb].

The rationale behind biodegradable stents can be simply explained in the wonderful allegory of Lucius Quintius Cincinnatus by Colombo and Karvouni in their 2000 *Circulation* editorial: a "biodegradable stent fulfills the mission and steps away" [COa]. Because development of restenosis usually happens during the first six months after deployment [KIa, KAb], a permanent prosthesis that is in place beyond this initial period has no clear function. However, it is worth recognizing that besides leading to unpredictable complications (e.g. stent failure due to fatigue, obstacles for other treatments, and infection due to the presence of a foreign body inside the lumen), there are no demonstrable clinical complications with a permanent intracoronary stent. Thus, the question should be turned around and one should ask what the advantages of a temporary stent are [COa]. The answer is manifold: (1) if a stent degrades and is absorbed by the body it will not be an obstacle for future treatments; (2) if a stent degrades in a controlled manner, its desired failure can be predicted and prescribed; (3) also, the gradual softening of the stent would permit a smooth transfer of the load from the stent to the healing wall; (4) because of the viscoelastic behavior of most polymers, a nonchronic deployment could be designed, preventing arterial injury inherent to balloon inflation; and (5) a biodegradable stent may act as an optimal vehicle for specific therapy with drugs or genes.

Also, there are some drawbacks with regard to permanent metal stents that biodegradable stents would not have. Metal stents remain inside the body indefinitely, becoming a potential nidus for infection [THa], and can be an adverse obstacle for subsequent treatments making bypass surgery almost the only hope for treatment of in-stent restenosis [AGb]. A significant challenge in the development of a novel biodegradable stent is the lack of precise engineering modeling tools [BLa].

Essentially, three different steps are usually taken in the design of such devices. First, only a limited number of biodegradable materials have been tried, and in many cases the materials are picked based on the designer's past experience [STa, HAb]. Scant data are available on the mechanical behavior of polymers during degradation. In most studies, emphasis is given to chemical quantities or phenomenological measurements. Examples are

the temporal evolution of molecular weight distribution (MWD) and quantification of mass loss over time. This results in a considerable amount of uncertainty with regard to the design of a biodegradable stent. Secondly, the usual procedure is to pick pre-existing stent designs and manufacture them with biodegradable materials. There are some concerns with manufacturing and sterilization of these polymeric devices when compared with stainless steel counterparts because polymers cannot usually be processed using metal stent techniques [GRb]. Also, the usual forms of solid polymers are fibers, films, or matrices. From these building blocks, the stent must be woven or assembled. The sophistication of the existing designs is variable, ranging from the simplest single fiber helicoidal stents [VAa] to the more complex interwoven stents [GRb, UUa, SUa]. The last step is then to conduct experiments, either in vivo [HIa, UNa], or in vitro [AGb, ZIb], analyze the results, and draw conclusions. Computational simulations with biodegradable stents are either nonexistent or simplistic in virtue of the inability to account for the complexity of the constitutive modeling. Grabow et al. used a finite element analysis to investigate the mechanical properties of a balloon-expandable PLLA stent under various load conditions, whereas Nuutinen et al. used an analytical method for calculating the mechanical properties of braided stents [GRa, NUa]. Both models consider the polymer as being a linearized elastic material with no effect due to the degradation being taken into account.

Because of this inductive way of dealing with the problem, the number of materials and designs used in biodegradable stents is as large as the number of people working in the field. Certain main trends can be identified: (1) biodegradable stents made of bioerodible metals, for example, magnesium [HEa, DIa], are currently in use (a choice that evolved from corrodable iron [PEb]), (2) natural polymers such as type I collagen were used to make tubes [BIa], and lastly, (3) a somewhat large number of biodegradable polymers were tried, more commonly aliphatic polyesters (e.g. polyglycolic acid and polylactic acid) [PEa, VEc]. Poly-L-lactic acid is probably the most commonly used of all these polymers. It was used for the Duke stent [AGb, AGa, LAa], and is being used in the Igaki–Tamai stent [TAb, TAc, TSa, TSb], by Eberhart et al. in their biodegradable stent [YEa, SUa, ZIb, ZIc], and in the Tampere stent for urethral applications [UUa, TAd, ISa]. Unfortunately, almost all of these previous studies focused on the chemical aspects of degradation and not in the mechanical changes occurring during degradation. Regardless of the material that the stent is made of, the issue of structural integrity is the most important for its performance. Structural collapse can take place if weakness occurs in particular regions, so understanding the impact of degradation on local mechanical properties should be the ultimate goal of biodegradable stent design. Obviously, this question does not have an easy answer. Lastly, drug

delivery modeled with diffusion kinetics is another important aspect that needs to be addressed and is closely related with degradation, erosion, and mechanical response.

4.3 Degradation, Erosion, and Elimination

The number, availability, and utilization of synthetic biodegradable polymers has increased dramatically over the last 50 years, with applications ranging from the field of agriculture to biomedical devices. The first reported biomedical application of biodegradable polymers was absorbable sutures in the 1970s [LAd], and this remains today to be the most widespread use of this family of materials. After 30 years of growth and development, many other devices have become available to the practicing surgeon. Absorbable internal fixation devices for orthopedic surgery, such as pins, screws, suture anchors, and osteosynsthesis plates [PIb]. Biodegradable polymers have been chosen to be the optimal carriers for local drug delivery [LAc] and are widely used in tissue engineering applications [LEb]. The interest in these applications continues to increase as the number of biodegradable polymers evaluated with respect to the concept of biomaterials increases [VEb]. However, the number of compounds having reached the stage of clinical and commercial applications is still small [KHa].

Basically, one can distinguish between the two major applications for biodegradable polymers in the medical field. When used for prosthetic purposes, the contribution of the polymer is required for a limited period of time, especially the healing time, and the polymer can be engineered to degrade at a rate that will transfer load to the healing bone [ATa]. Also, there is no need for a second surgical event for removal [MIa]. To accomplish all of these requirements, the main concern behind the design of the device is its load-bearing capabilities as well as its evolution during degradation over time. On the other hand, for drug delivery implants, the attention is shifted to delivery kinetics and their changes during degradation. The case of a biodegradable drug eluting stent is a bridge connecting the two approaches. The stent must perform mechanically, maintaining the artery patent after deployment and during degradation, and be capable of effective drug delivery.

It is important to make distinctions between the terminologies often encountered in the literature. Biodegradable polymers are polymers that are decompose in the living body but whose degradation products remain in the tissues long-term. On the other hand, bioresorbable polymers can be defined as polymers that degrade after implantation into nontoxic products

which are then eliminated from the body or metabolized therein. Although this last term is more precise, it is often used interchangeably with other terms, including absorbable, resorbable, bioabsorbable, and biodegradable [HAb].

In their book, *Biodegradable Polymers and Plastics*, Ottenbrite et al. present a discussion aimed at settling the terminology for such polymers. The conclusion of the discussion board was a set of working definitions. Polymer degradation is a deleterious change in the properties of a polymer due to a change in its chemical structure. A biodegradable polymer is a polymer in which the degradation is mediated at least partially by a biological system. Also, a distinction between degradation and erosion was made. Degradation, defined as the change in chemical structure, is a process different from erosion, defined to be the process of dissolution or wearing away of a polymer [OTa]. Thus, a bioabsorbable polymer automatically implies degradation mediated by a biological system as well as its erosion into nontoxic byproducts that will be then absorbed by the body.

More precisely, polymer degradation is the chain scission process that breaks polymer chains down to oligomers and finally monomers. Degradation leads to erosion, which is the process of material loss from the polymer bulk. Such materials can be monomers, oligomers, parts of the polymer backbone, or even parts of the polymer bulk. Thus, degradation and erosion are distinct but related processes [PIa]. It is worth noting that all polymers undergo backbone chain scission; that is, all polymers "degrade." Only the time they require for degradation is different, and it can range from hours in the case of the hydrolytic degradation of poly-anhydrides, to many years for poly-amines [GOc]. The relationship between the actual life of the polymer and the intended life to perform its function will ultimately dictate the distinction between a polymer being degradable or nondegradable.

Polymers degrade by several different mechanisms, depending on their inherent chemical structure and on the environmental conditions to which they are subjected. Degradation results from an irreversible change of the material which eventually leads to its breakdown or failure. There are five major mechanisms of polymer degradation: thermal, radiation induced, mechanical, enzymatic, and chemical [GOb].

Covalent bonds of the backbone chain of the polymer have a limited strength. In thermal degradation, scission is due to the highly excited vibrational state of bonds attained with increases of temperature. When the energy associated with the vibrational state overcomes the bond dissociation energy, scission and consequently degradation occur. Although these processes cause rapid decomposition of polymers only at highly elevated temperatures (around 500°C), the pronounced temperature dependence of the rates of chemical reactions can cause a significant and rather rapid

degradation already under milder conditions [WEb]. Radiation induced degradation occurs when polymers undergo chemical reactions upon irradiation with ultraviolet light or gamma radiation [SCd]. In general isothermal biomedical applications, such as the use of endovascular biodegradable stents, thermal degradation and radiation-induced degradation are not assumed to be relevant.

Mechanical degradation of polymers comprises a large number of different phenomena, ranging from fracture to chemical changes induced by the mechanical environment. Mechanical energy transferred to a polymeric system can be dissipated via two main relaxation processes: enthalpy relaxation, defined to be the slippage of chains relative to surrounding molecules, and entropy relaxation, changes of chain conformation. These relaxations are harmless to the polymer because they do not induce chemical changes. In competition with these relaxation processes, the scission of chemical bonds can occur. Obviously, the probability for bond scission should increase as relaxation is impeded. A single, generally applicable mechanism of stress induced chemical reactions does not appear to exist. It seems that different bond scission mechanisms are operative depending on the state of the polymer (solid, rubbery, or molten) and the mode of imposition of stress. In solid polymers, fracture planes and voids might give rise to the rupture of chemical bonds. In the rubbery state or molten in solution, inter- and intrachain entanglements might cause stretching of parts of the macromolecules, resulting eventually in bond scission. Strain is a prerequisite for bond rupture in polymer chains regardless of the state of the material; that is, bond rupture occurs when sufficient energy is concentrated in a certain segment of a macromolecule as a consequence of the nonuniform distribution of internal stresses [SCd].

Enzymatic degradation is mainly relevant for natural polymers such as proteins, polysaccharides, or poly β-hydroxy esters, for which specific enzymes exist [GOc]. Chemical degradation is a general classification of molecular weight reduction due to chemical reactions that start spontaneously when certain low molecular weight compounds are brought in contact with the polymer [SCd]. Hydrolysis and oxidation are classic examples of chemical degradation.

The prevailing mechanism of biological degradation for synthetic biodegradable polymers is scission of the hydrolytically unstable backbone chain by passive hydrolysis, because for most of them, no specific enzymes exist [WEa]. By tailoring the polymer backbone with hydrolyzable functional groups, the polymer chains become labile to an aqueous environment and their ester linkages are cleaved by absorbed water [HAa]. There are several factors that influence the rate of this reaction: the type of chemical bond, pH, co-polymer composition, and water uptake are the most important [GOb]. Other factors can also be relevant: residual monomer

concentration [HYa], autocatalysis [SId], temperature [WEb], chemical environment [ZHa], and initial molecular weight [IVa], just to name a few. On the other hand, one must realize that although the number of factors that influence the degradation of polymers might be infinite, under the conditions of interest only some might be relevant. Moreover, inherent chemical and physical changes to the polymer and to the surrounding environment might have a substantial feedback on the degradation rate [GOc].

For semi-crystalline polymers, hydrolysis occurs in two distinct stages: initially, water penetrates the polymer, preferentially attacking the more accessible chemical bonds in the amorphous phase and converting long polymer chains into shorter, ultimately water-soluble fragments [GOb]. Because the amorphous phase is degraded in the first place, there is a reduction in molecular weight without a loss of apparent physical properties as the polymer matrix is still held together by the crystalline regions. The reduction in molecular weight is soon followed by a reduction in physical properties as water begins to fragment the polymer bulk [ALb, ALc].

The diffusion of water into the polymer bulk and polymer degradation compete against each other in the process of polymer erosion. If degradation is fast, the diffusing water is absorbed quickly by hydrolysis and hindered from penetrating deep into the polymer bulk. In this case, degradation and consequently erosion are restricted to the surface of the polymer, a phenomenon referred to as heterogeneous or surface erosion [TAa]. This type of erosion changes if degradation is slower than the rate of diffusion of the water through the polymer. In this case water cannot be absorbed quickly enough to be hindered from reaching deep into the polymer and the polymer degrades and erodes through its cross-section, a behavior which has been termed homogeneous or bulk erosion [TAa]. It must be stressed, however, that surface and bulk erosion are two extremes and the erosion mechanism in a degradable polymer usually shows characteristics of both.

In addition to water diffusion and bond stability, other factors such as water uptake which depends on the hydrophilicity of the polymer affect the hydrolysis rate and the erosion behavior of polymers substantially [BUa]. As should be expected, many different types of morphological changes occur upon erosion. An increase in surface roughness and the formation of cracks, macropores, and micropores are common phenomena observed in degrading polymers. Erosion fronts, which separate eroded from noneroded polymer, have been reported for surface eroding polymers such as poly(anhydrides) [KAc]. In contrast, inversely moving erosion fronts have been observed in poly(DL-lactide) [LIa], where polymer degradation is increased inside eroding polymer matrices due to the autocatalytic activity of monomers that have been created [SId]. Due to the preference for the amorphous phase, the degree of crystallinity of degradable polymers can change tremendously

during erosion [PIc]. Additional changes in crystallinity are a consequence of the recrystallization of oligomers and monomers [LIb].

Elimination is the concluding stage of the complete function of a biodegradable implant. The obvious requirement is to have a polymer that is biocompatible during the whole time of permanence inside the body as well as its breakdown products being eliminated through metabolism in a nontoxic manner [ZIa]. The biocompatibility of aliphatic polyesters, especially polyglycolic and polylactic acid, is well established in the literature [SCa, PId, NGa]. On the other hand, the elimination of the byproducts of degradation and erosion appears to follow different mechanisms for different polymers and is controversial. Ultimately, the elimination involves the solubilization of the degradation products which are then carried away from the implantation site and eliminated [KAc]. The surrounding tissue (in the case of a biodegradable stent, the artery wall) must be capable of absorption, digestion, and elimination of the resulting oligomers and monomers [GUa]. The last step is the removal of these waste products from the blood. Lysosomal degradation is the major pathway for the elimination of polymers that cannot be excreted directly via the kidney [WIa].

4.4 Models of Degradation and Erosion

Theoretical models to predict polymer degradation and erosion would seem to be important tools for a number of different applications. If drug elution is to be part of the therapy, drug delivery profiles should be programmable at the design stage. For orthopedic applications, load-bearing capabilities as well as their evolution with time must be determined. A drug eluting biodegradable stent should ideally be designed accounting for all of these criteria.

Hydrolysis degradation is the breakage of backbone bonds caused by incoming water and is a phenomenon that occurs at the molecular level [VEa]. It is a very intricate process, as a variety of different degradation mechanisms can occur simultaneously and concurrently. Also, the reactivity of each bond might be equal when considered individually, but the large number of repeating units and their inherent steric environment, weak links, and branches, may influence the local rate of reaction [NGb]. The probability of hydrolysis and consequent scission of a particular bond is expressed as a distribution function (commonly random scission, central Gaussian and parabolic). Monte Carlo or other more complex techniques are applied to populations of simple polymers to predict the theoretical evolution of MWD [NGb]. Experiments with gel permeation chromatography

provide data to model the mechanism of degradation [NGc]. Other degradation models based on kinetics have been reported [BRa, BEb]. Lastly, complex degradation schemes depicting possible mechanisms can be developed and computationally solved to obtain realistic MWD evolutions [BOa, YOa].

Erosion is the dissolution of oligomers and monomers resulting from degradation. Joshi and Himmelstein [JOa] proposed a reaction-diffusion model for degradation and drug release, consisting of Fick's law of diffusion coupled with a reaction equation describing the kinetics of the degradation mechanism. Theoretical results for drug release, water penetration, and erosion were obtained as a consequence of degradation and were corroborated with experimental results [JOa, THb]. One drawback of this model is that it does not take into account changes in the microstructure caused by the preferential erosion of the amorphous phase compared with crystalline phase.

Gopferich and Langer developed different models for erosion [GOa]. They describe erosion as being a probabilistic event and the polymer matrix as a grid of pixels. Monte Carlo simulations coupled with a reaction equation describing random scission were performed. Different properties can be assigned to each pixel, so a distinction between the crystalline and amorphous phase was considered. By removing eroded pixels continuously from the grid, temporal evolutions of a degradable polymer matrix can be determined stochastically. From such simulations, many experimentally measurable parameters can be calculated, such as porosity or weight loss. Erosion fronts and erosion modes can also be inferred from the results of the simulation. The fit of experimental data allows the determination of the erosion rate constants and demonstrates that the stochastic model is quite well able to adjust to the experimental data. Later models by the same group included diffusion equations to obtain theoretical results on the release of drugs through the pores [SIa].

Up until now, most of the research effort on biodegradable polymers were directed experiments and product development. A fair amount of experimental data concerning biodegradable polymers exists, ranging from MWD evolutions, mass loss, and amount of drug eluted. Because of the complexity of these materials and the variety of processes to which they are subjected, the modeling effort has been very limited. The existing models are based on widely different approaches, certainly driven by the field of application. Drug delivery and erosion for drug delivery implants are far better understood when compared to the impact of degradation on the load-bearing performance in orthopedic applications, usually based on phenomenological models with data from in vitro and in vivo experiments. We were not able to identify any previous study of the impact of degradation and erosion on the mechanical response of polymers.

As can be expected, the biodegradation of the polymers that constitute a stent depend on two classes of factors: the mechanical environment and the biochemical environment. One could easily imagine an astonishingly large number of parameters in these broad categories that potentially could influence the degradation, ranging from stress or strain on a strut to the concentration of a particular compound present in the blood. Besides degradation modeling (how the polymer chains are broken) and erosion modeling (how monomeric and oligomeric products are washed out), the modeling of the mechanical response is equally relevant. To know how the degradation influences the mechanical response requires significant effort. The next sections outline our initial modeling efforts, which are aimed at developing a tool for biodegradable stent design.

4.5 Model Description

As mentioned earlier we introduce a measure of the degradation through a field $d(\mathbf{x}, t)$, which we refer to as the degradation field. It is a scalar field defined over the body and is assumed to be positive. It reflects the bond scission of the polymer backbone chains and results solely in molecular weight reduction. One can think of degradation as a measure of the density of broken bonds. Another important assumption is that degradation should be a consequence of bond scission and the factors on which it depends. Degradation is assumed to depend on the strain field and time and only mechanical degradation is described by our model. We define the evolution of the degradation through

$$\frac{\partial d(\mathbf{x}, t)}{\partial t} = \hat{D}(\boldsymbol{\epsilon}, t), \tag{5.1}$$

where $\boldsymbol{\epsilon}$ is the linearized strain. In a problem involving large strains, we use a nonlinear measure of strain such as the Almansi–Hamel strain. This relation reflects the mechanism of scission caused by strain and describes mechanical degradation.

The rationale for the choice of (5.1) for the evolution of the degradation field is the following: (1) a material degrades faster when exposed to higher strains, and (2) a material that is strained for a longer period of time degrades more rapidly than a material that has been strained by the same amount for a shorter period of time. In other words, materials subjected to larger strains, other things being held equal, degrade faster; and materials subjected to the same strain for a longer time, other things being held equal, degrade faster [RAa]. Obviously, this behavior depends on the

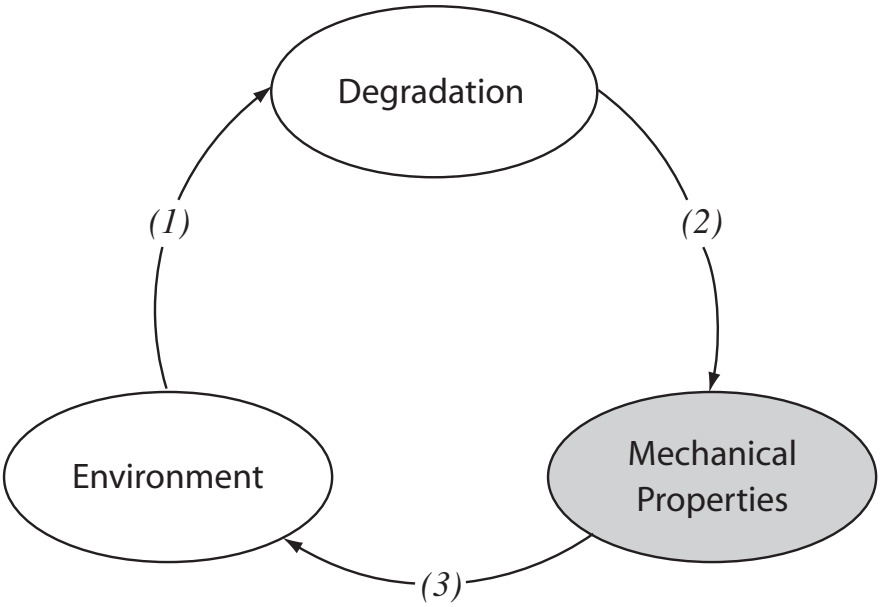

Figure 4.1. General pathway of strain induced degradation. A material degrades depending on the strain to which it is subjected (1). As degradation proceeds its mechanical properties decrease (2), leading to a new equilibrium position (3) that will be responsible for more degradation (1).

choice of $\hat{D}(\boldsymbol{\epsilon}, t)$. Examples of mechanical degradation are common. Aging processes, ultrasonic degradation, stress induced chemical alterations of polymers, and mastication of rubber can be described through these mechanisms. The closed loop cause–effect mechanism of degradation is shown in Figure 4.1.

The body was considered to be a linearized elastic body when degradation was absent. Although this simple model does not describe polymeric materials undergoing large deformations, the choice of this model was made based in virtue of the simplicity of the governing equations that it yields. The methodology can certainly be extended to the finite deformation case, as will be necessary for a fully realistic model of a stent. For the same reasons, a simple geometry was chosen in order to obtain an easy mathematical problem. The classical linearized elasticity solution of a cylindrical pressure vessel was chosen in order to obtain a problem that involves only one spatial variable. The cylindrical model is representative of stent geometries, and provides a means to obtain results in a tractable framework. Incorporation of this model into a finite element code would allow for more complex geometries to be modeled.

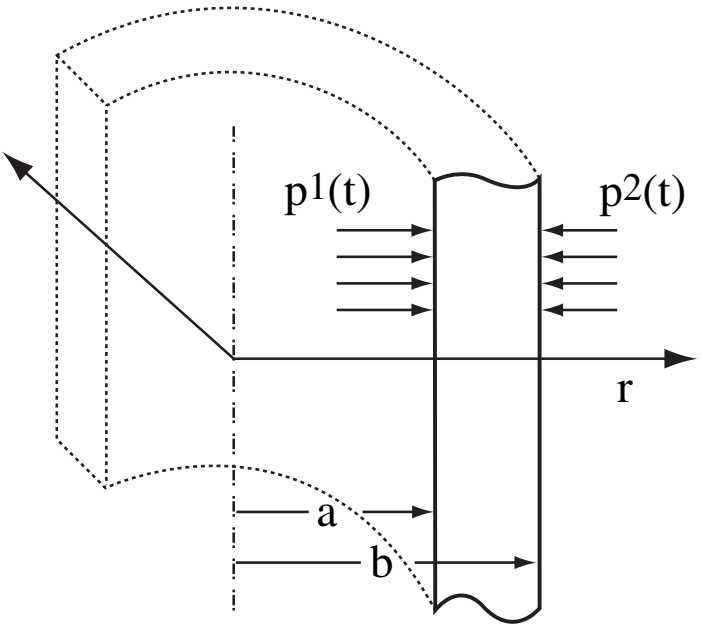

Figure 4.2. Geometry of the body considered.

Consider an infinitely long, homogeneous, isotropic, elastic cylindrical annulus described by the classical linearized theory with inner and outer radii a and b, respectively, under radial pressure at both the inner and outer surfaces as shown in Figure 4.2. A semi-inverse method can be used to solve this simple classical linearized elasticity problem. We assume that

$$\mathbf{u} = u(r,t)\mathbf{e_r}. \tag{5.2}$$

The linearized strain $\boldsymbol{\epsilon}$ is defined by

$$\boldsymbol{\epsilon} = \frac{1}{2}\left(\nabla\mathbf{u} + \nabla\mathbf{u}^{\mathbf{T}}\right).$$

In this problem, there are only two nonzero components of the strain tensor (expressed in cylindrical polar coordinates defined along the cylindrical annulus).

$$\epsilon_{rr} = \frac{\partial u}{\partial r}, \tag{5.3}$$

$$\epsilon_{\theta\theta} = \frac{u}{r}. \tag{5.4}$$

The stress field $\boldsymbol{\sigma}$ can be computed in terms of two material parameters. In this case, the Young's modulus E and the Poisson ratio ν are used and

the constitutive relation takes the form

$$\boldsymbol{\sigma} = \frac{E}{1+\nu}\boldsymbol{\epsilon} + \frac{E\nu}{(1+\nu)(1-2\nu)}(\text{tr }\boldsymbol{\epsilon})\mathbf{I}. \tag{5.5}$$

Only three components of the stress tensor are different from zero, σ_{rr}, $\sigma_{\theta\theta}$, and σ_{zz}. Substituting (5.3) and (5.4) into (5.5), the stresses are given by

$$\sigma_{rr} = \frac{E\nu}{(1+\nu)(1-2\nu)}\left[(1-\nu)\frac{\partial u}{\partial r} + \nu\frac{u}{r}\right], \tag{5.6}$$

$$\sigma_{\theta\theta} = \frac{E\nu}{(1+\nu)(1-2\nu)}\left[(1-\nu)\frac{u}{r} + \nu\frac{\partial u}{\partial r}\right], \tag{5.7}$$

$$\sigma_{zz} = \frac{E\nu}{(1+\nu)(1-2\nu)}\left(\frac{\partial u}{\partial r} + \frac{u}{r}\right). \tag{5.8}$$

The balance of linear momentum yields the equation

$$\text{div }\boldsymbol{\sigma}^T + \rho\mathbf{b} = \rho\frac{\partial^2\mathbf{u}}{\partial t^2}. \tag{5.9}$$

The density ρ was assumed not to change during degradation. This assumption can be supported by experimental data on bulk erosion. Degradation takes place over the entire body and only after some time erosion mechanisms are triggered [PIa]. Before that happens, backbone chain scission can be assumed to happen without mass loss. This once again stresses the difference between degradation and erosion. Using the predetermined stress field (5.6)–(5.8) in the local form of the momentum balance (5.9) and assuming no body forces, the only remaining nontrivial component is the radial component, which simplifies to

$$\frac{\partial\sigma_{rr}}{\partial r} + \frac{\sigma_{rr} - \sigma_{\theta\theta}}{r} = \rho\frac{\partial^2 u}{\partial t^2}. \tag{5.10}$$

The degradation field $d(\mathbf{x}, t)$ is assumed to depend only on the radial position and time, $d(r, t)$. This field quantifies the progress of degradation of the material at each current location. It can only assume positive values without any upper bound and if it is zero it means no degradation has taken place.

To model a biodegradable polymer, the parameters describing the mechanical properties are allowed to decrease as degradation progresses. An equation relating the decrease in the mechanical properties with the increase of degradation is assumed. In this model, it was assumed that only the Young's modulus of the material decreases during degradation in the following manner,

$$E(r, t, d) = E_0[1 - \beta d(r, t)], \tag{5.11}$$

where E_0 is the Young's modulus associated with the virgin specimen and β is a constant that weights how the degradation field leads to a reduction of the mechanical properties. The Poisson ratio was assumed to be constant with a value close to that for an incompressible body ($\nu = 0.49$), so as to reflect the near constant density of the polymeric materials under consideration. Then, the constitutive equation (5.5) assumes the form

$$\boldsymbol{\sigma} = \frac{E(r,t,d)}{1+\nu}\boldsymbol{\epsilon} + \frac{E(r,t,d)\nu}{(1+\nu)(1-2\nu)}(\text{tr } \boldsymbol{\epsilon})\mathbf{I}. \tag{5.12}$$

To relate the increase of degradation to the mechanical stimuli to which the body is subject, the equation that governs the degradation (5.1) is assumed to be of the following form,

$$\frac{\partial d(r,t)}{\partial t} = D(t)\epsilon_{\theta\theta}, \tag{5.13}$$

where $D(t)$ is a strain degradation parameter. Generally speaking, the rate of increase of degradation is assumed to be dependent solely on the linearized strain. Due to incompressibility, the dilation (the trace of the linearized strain tensor) is approximately zero. Thus, because of particular characteristics of the strain field of a pressurized cylindrical annulus (i.e. plane strain), ϵ_{zz} is zero and $\epsilon_{\theta\theta}$ and ϵ_{rr} add up to zero. For this problem, the degradation was simplified to be dependent on just one component of the strain field, more precisely the hoop strain $\epsilon_{\theta\theta}$. Also, it is assumed that the rate of increase of degradation would have the separable representation shown in (5.13).

Introducing the stress field (5.6)–(5.8) together with (5.12) into the balance of linear momentum (5.10) yields a second-order partial differential equation

$$A_1 u_{rr} + A_2 u_r - A_3 u = \rho u_{tt} \qquad a < r < b, t > 0, \tag{5.14}$$

where each letter subscript represents a partial derivative with respect to that variable. The coefficients A_1 through A_3 depend on the degradation field through the following expressions.

$$A_1 = \frac{E_0(1-\nu)}{(1+\nu)(1-2\nu)}[1-\beta d], \tag{5.15}$$

$$A_2 = \frac{E_0(1-\nu)}{(1+\nu)(1-2\nu)}\left[\frac{1-\beta d}{r} - \beta d_r\right], \tag{5.16}$$

$$A_3 = \frac{E_0(1-\nu)}{(1+\nu)(1-2\nu)}\left[\frac{\nu}{1-\nu}\frac{\beta d_r}{r} - \frac{1-\beta d}{r^2}\right]. \tag{5.17}$$

Substituting the hoop strain (5.4) into the equation governing the degradation (5.13) yields

$$d_t = \frac{D(t)}{r}u. \tag{5.18}$$

Equation (5.14) is a nonlinear hyperbolic PDE. The nonlinearity arises from the dependence of the Young's modulus on the degradation field. Equation (5.18) is parabolic. Both must be solved for $d(r,t)$ and $u(r,t)$ simultaneously. Traction boundary conditions are imposed on both surfaces of the annulus:

$$\begin{cases} \sigma_{rr}|_{r=a} = -p_1(t) \\ \sigma_{rr}|_{r=b} = -p_2(t) \end{cases} \qquad t > 0. \tag{5.19}$$

Initial conditions on the displacement and degradation fields must be specified. They are:

$$\begin{cases} u|_{t=0} = 0 \\ \dot{u}|_{t=0} = 0 \\ d|_{t=0} = 0 \end{cases} \qquad a < r < b \tag{5.20}$$

with the understanding that the annulus is at rest and nondegraded initially.

4.6 Methods

Because of the nonlinear nature of the resulting partial differential equations, a time marching nonlinear finite element scheme with a set of nonlinear iterations for each time step was implemented to simultaneously solve both equations (5.14) and (5.18) for the unknown functions $u(r,t)$ and $d(r,t)$, subject to the boundary conditions (5.19) and the initial conditions (5.20). The infinitely long cylindrical annulus was modeled to simulate a stent deployed inside a coronary artery (shown in Figure 4.2). The outer radius, b, was chosen to be 2.5 mm, and represents an average coronary artery. Considering a typical strut thickness of 100 μm, the inner radius, a, was chosen to be 2.4 mm. Pressure applied on the inner surface of the annulus, $p_1(t)$ in (5.19), was chosen to simulate the pressure during blood flow. A steady pressure field of 13 kPa ($\approx$ 98 mmHg) was superimposed with an oscillatory component with an amplitude of 2.75 kPa, yielding a systolic and diastolic pressure of 118 mmHg and 77 mmHg respectively. The frequency was taken to be 1 beat per time unit, simulating resting conditions.

The outer pressure, $p_2(t)$ in (5.19), representing the crushing action of the artery in the stent after deployment, was taken to be constant and with value of 202 kPa (2 atm). This value was based in a 3-D finite element model of the deployment of a metal stent in a hyperelastic coronary artery [BEa]. The mechanical properties chosen were for PLLA assuming a linear elastic behavior. PLLA is generally incompressible, so a Poisson ratio ν of 0.475 was chosen. The nondegraded Young's modulus E_0 in (5.11) was assumed

to be 3.5 GPa, according to published data obtained from experimental results [DRa, GAb, LUa].

The domain of the problem was meshed with 1-D Lagrangian quadratic elements. Mesh convergence was verified and 20 elements were chosen, being the best compromise between precision and a fast computational running time.

This problem deals with two completely different time scales. The frequency of the oscillatory component of the inner pressure is one sinusoidal cycle per time unit. The degradation, on the other hand, varies over days, months, or even years. The time march was performed through 25 time units. Although any degradation over this time interval is completely non-physical, the main purpose of this analysis was to understand the role of the degradation constants β and $D(t)$ on the degradation process (cf. Eq. (5.11) and (5.13)). A time step of 0.05 seconds was chosen. This time step was enough to assure stability of the time marching scheme.

Two types of data were analyzed. From one standpoint, temporal evolutions of important quantities at a given point in the spatial domain were obtained, for example, the displacement of the inner surface of the annulus as a function of time, or the variation of the three nonzero components of the stress field at the outer surface. On the other hand, fields can be plotted along the entire domain at a given moment in time, and the evolution of the fields considered can be characterized.

As a starting point, a representative problem was studied with the degradation parameters taken to be $\beta = 5$ and $D(t) = 1$. Then, a parametric analysis was performed with regard to these two representative parameters. Three more cases were considered to study the effect of β, one lower ($\beta = 1$), and two greater ($\beta = 10$ and $\beta = 20$). The study on the influence of $D(t)$ in the degradation was done in two distinct steps. Firstly, three more constant $D(t)$ were considered, $D(t) = 2.5$, $D(t) = 5$, and $D(t) = 10$. Then, to have a greater insight on the role of $D(t)$ on the degradation mechanism, several shapes were considered and are shown in Figure 4.3. Table 4.1 shows schematically the cases considered.

To access the effects of the thickness of the annulus on the degradation process, two additional geometries besides the one considered in the representative case above were considered. The parameters of degradation, boundary conditions, and initial material properties were kept constant, and an aspect ratio, defined to be the ratio of the outer radius to the thickness of the annulus (i.e. $b/(b-a)$), was varied and is systematized in Table 4.2.

Lastly, to assess the influence of the applied loads on the degradation of the annulus, a different type of analysis was performed. The outer pressure was cycled between the inner pressure and 202 kPa considered in all of the previous cases. Four linear loading and unloading cycles over 100 time

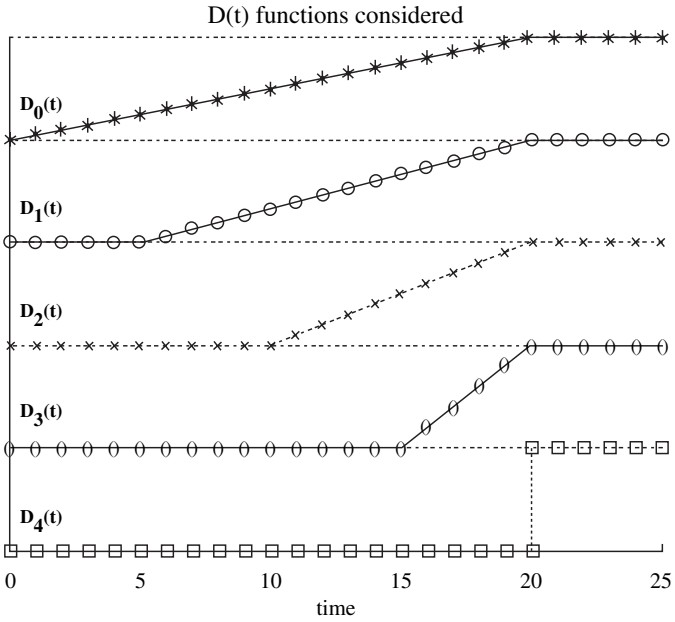

Figure 4.3. Shapes of several $D(t)$ considered. Ultimately, all will end with the same $D(t) = 1$. $D(t) = 0$ yields no degradation.

units were considered. Two different sets of degradation parameters were analyzed, $\beta = 5$, $D(t) = 1$ and $\beta = 10$, $D(t) = 2$.

4.7 Results

As time increases and degradation proceeds, the overall value of the radial displacement of the cylindrical annulus increases at a progressive rate, that is, the annulus creeps inwards when subjected to the same loads (Figure 4.4). For this initial representative case ($\beta = 5$ and $D(t) = 1$; cf. Table 4.1), the inner displacement increases 0.4 μm over 25 time units, a 15% increase when compared with the nondegraded radial displacement.

Due to the kinematical characteristics of this deformation and the strain field that it causes, a slightly inhomogeneous increase in degradation is observed (Figure 4.5). The inner part of the annulus is subjected to greater strains and therefore to a stronger degradation. This degradation has consequences on the material properties and the Young's modulus decreases steadily through the thickness as degradation and time increase. At the inner surface, where the degradation is more intense, a reduction of

	β	$D(t)$
Representative Case	5	1
Parametric Study		
Influence of β	1	1
	5	
	10	
	20	
Influence of $D(t)$	5	1
		2.5
		5
		10
Influence of the shape of $D(t)$	5	D0
		D1
		D2
		D3
		D4

Table 4.1. Summary of the cases considered for the parametric study of the degradation parameters β and $D(t)$. The specific forms of the functions D0 through D4 are shown in Figure 4.2.

	a	**b**	**b/(b-a)**
Representative case (thin-walled annulus)	2.4	2.5	25
Medium thickness annulus	1.5	2.5	2.5
Large thickness annulus	0.5	2.5	1.25

Table 4.2. Summary of the cases considered for the parametric study of the degradation parameters β and $D(t)$. The specific forms of the functions D0 through D4 are shown in Figure 4.2.

approximately 15% in the Young's modulus after 25 time units is observed (Figure 4.6).

The linearized strain field follows the same behavior as the displacement. The radial strain $\epsilon_{rr}(r,t)$ is positive and the hoop strain $\epsilon_{\theta\theta}(r,t)$ has a negative value (Figure 4.7). All the other components of the strain field tensor in this cylindrical coordinate system are zero. The two nonzero

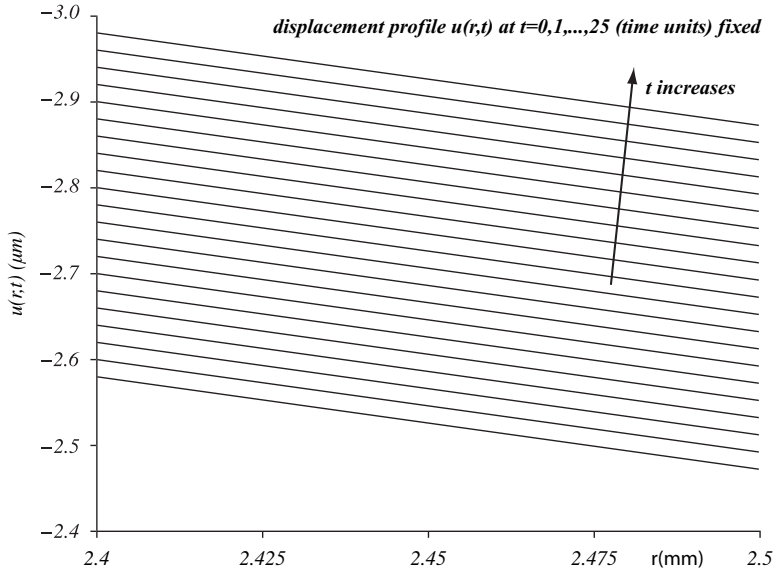

Figure 4.4. Displacement profiles $u(r,t)$ at $t = 0, 1, 2, \ldots, 25$ (time units). As time increases, the overall value of the displacement increases in absolute value with a progressive rate.

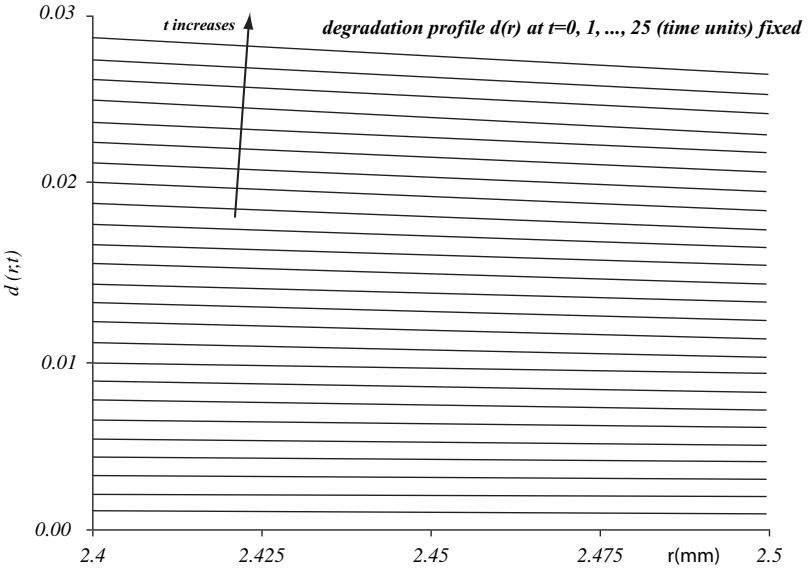

Figure 4.5. Degradation profiles $d(r,t)$ at $t = 0, 1, 2, \ldots, 25$ (time units). As time increases, the degradation increases. Degradation is nearly homogeneous, but is slightly more aggressive near the inner wall.

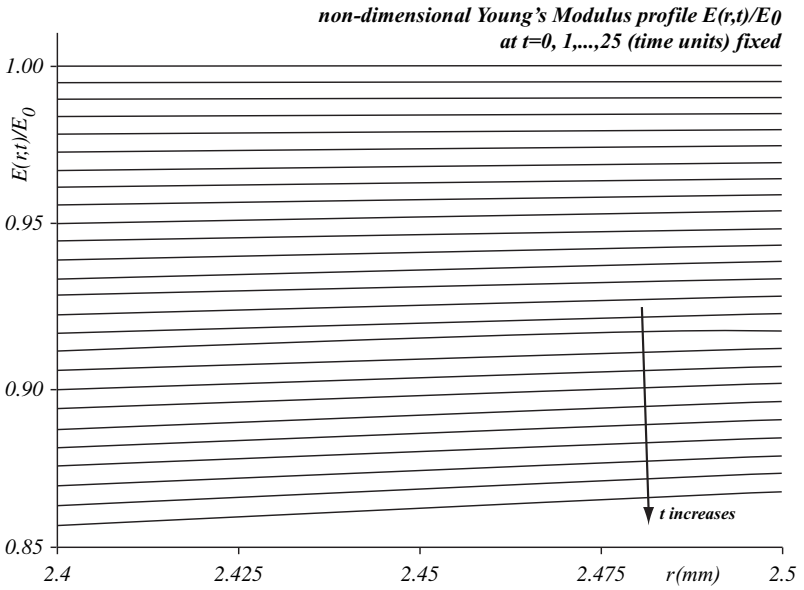

Figure 4.6. Nondimensional Young's modulus profile $E(r,t)/E_0$ at $t = 0, 1, 2, \ldots, 25$ (time units). The Young's modulus, initially constant throughout the thickness, shows radial dependence after the onset of degradation.

strains add up to approximately zero due to the near incompressibility of the material. Lastly, the values of the components of the linearized strain tensor are close to zero, thus the necessary requirement of small displacement gradients is verified.

Stress relaxation in the inner half of the annulus and an increase in the overall value of stress in the outer part are observed (Figures 4.8 and 4.9). Although both the hoop stress $\sigma_{\theta\theta}(r,t)$ and the axial stress $\sigma_{zz}(r,t)$ show significant differences from the classical linearized solution, stress relaxation and stress intensification are more relevant in the former than in the latter. An approximately 30 kPa relaxation in $\sigma_{\theta\theta}(r,t)$ at the inner surface and a similar increase in the outer part are observed (Figure 4.8). The axial stress departs from the constant through the thickness result obtained from the classical linearized solution, and the relaxation and intensification patterns are similar (Figure 4.9). However, the radial stress $\sigma_{rr}(r,t)$ shows little effect of degradation (Figure 4.10); due to the pressure boundary conditions, the whole radial stress profile is prescribed for all times.

4.7.1 On the Influence of the Load

Hysteresis loops are observed in the hoop stress $\sigma_{\theta\theta}(a,t)$ versus hoop strain $\epsilon_{\theta\theta}(a,t)$ diagram at the inner surface when the outer pressure is steadily

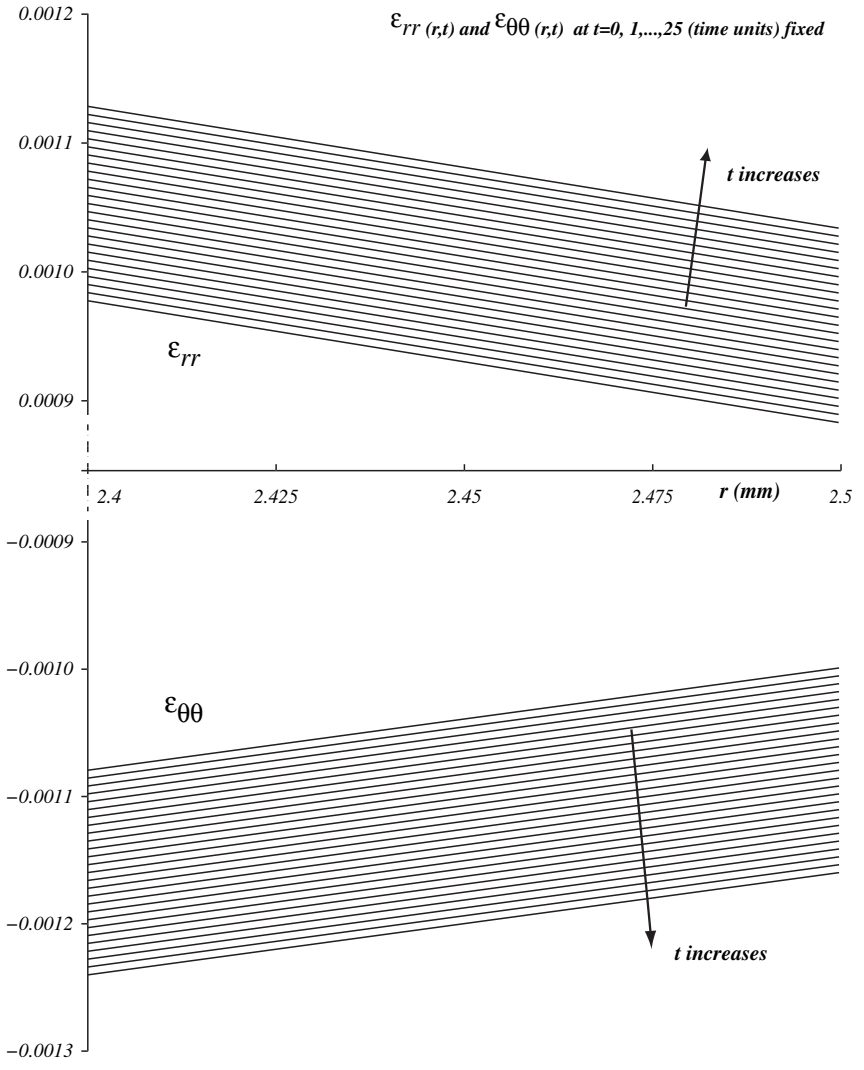

Figure 4.7. Strain field $\epsilon_{rr}(r,t)$ and $\epsilon_{\theta\theta}(r,t)$ at $t = 0, 1, 2, \ldots, 25$ (time units). The order of magnitude of the components of the infinitesimal strain tensor is small, therefore the assumption of linearized elasticity holds for this deformation.

cycled four times between the inner pressure and 202 kPa (Figure 4.11). Hysteresis is dependent on the degradation parameters, with the area spanned by the hysteresis loop increasing as degradation proceeds. Not only are the effects of degradation indistinguishable for the first cycle between

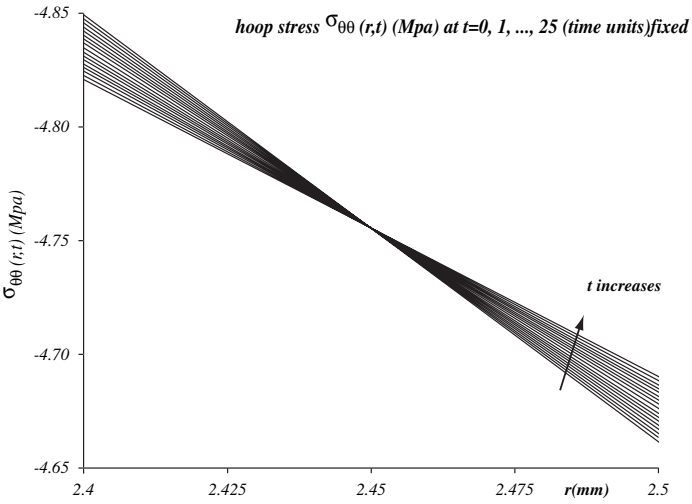

Figure 4.8. Hoop stress $\sigma_{\theta\theta}(r,t)$ at $t = 0, 1, 2, \ldots, 25$ (time units). Stress relaxation is observed in the inner half of the annulus. On the outer half, the stress increases in order to satisfy the linear momentum balance.

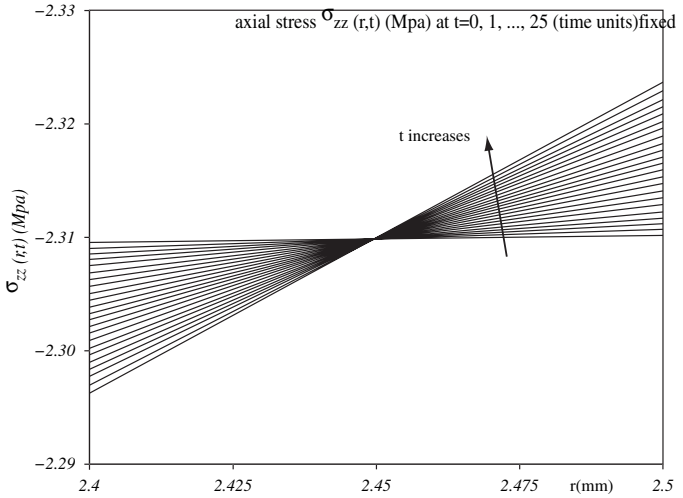

Figure 4.9. Axial stress $\sigma_{zz}(r,t)$ at $t = 0, 1, 2, \ldots, 25$ (time units). The nondegraded classical solution would yield a constant valued axial stress through all the annulus thickness. Due to degradation, relaxation occurs in the inner half.

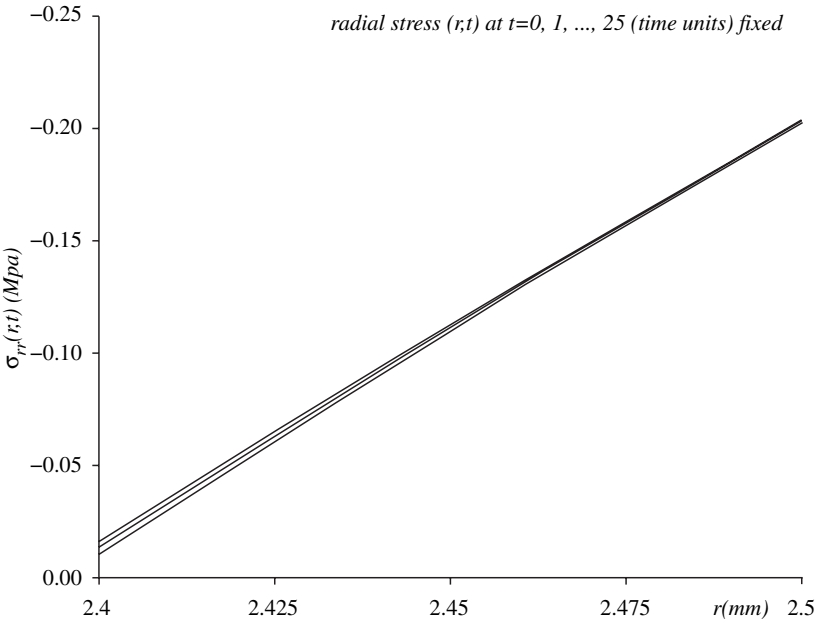

Figure 4.10. Radial stress $\sigma_{rr}(r,t)$ at $t = 0, 1, 2, \ldots, 25$ (time units). Due to BCs, 13 ± 2.75 kPa at the inner radius and 202 kPa in the outer radius, the whole profile is prescribed for all times.

the two sets of degradation constants, but also as degradation proceeds the curves deviate from each other. Lastly, no permanent set is induced due to the degradation imparted through this model; when the annulus is unloaded, it returns to its original configuration.

4.7.2 On the Influence of the Thickness of the Wall

The most important difference obtained through the different geometries referred to in Table 4.2 is the decrease of the homogeneity of the deformation. A deformation is said to be homogeneous if straight lines are mapped through the deformation into straight lines (or, if in a Cartesian coordinate system, the components of the deformation gradient are constants). In the case of a thin-walled annulus, the deformation is almost homogeneous, as can be inferred by the flatness of the displacement profile (Figure 4.12, first column). When the thickness of the annulus is increased, the deformation becomes more inhomogeneous, leading to a less flat radial displacement profile and consequently a more inhomogeneous degradation (Figure 4.12, second and third columns).

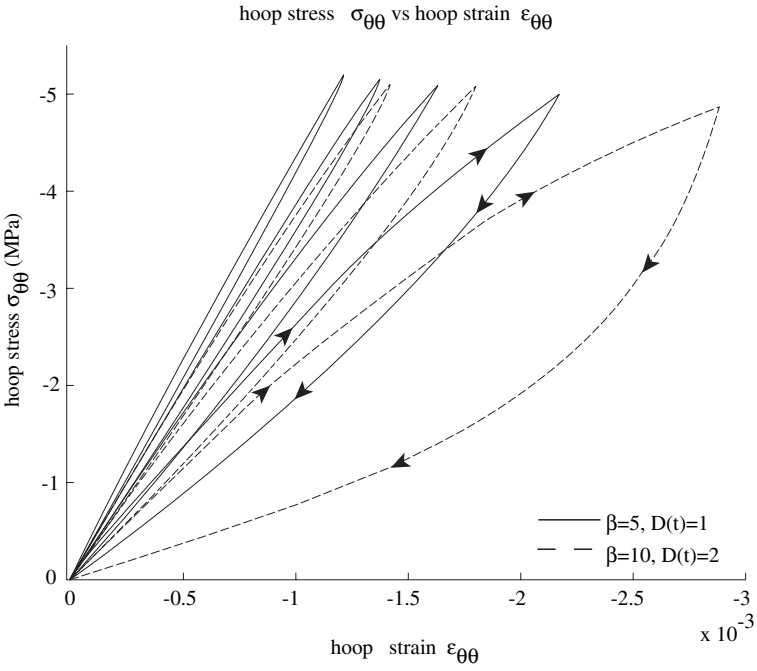

Figure 4.11. Hoop stress $\sigma_{\theta\theta}(a,t)$ versus hoop strain $\epsilon_{\theta\theta}(a,t)$ at the inner radius. The outer pressure $p_2(t)$ cycles four times between the inner pressure and 202 kPa. The loading/unloading curves are distinguished with arrows (shown only for the last cycle).

The radial displacement profile as well as its evolution show significant differences from the representative case: the nearly homogeneous deformation is lost, as well as the rate at which the annulus creeps inwards changes. An example of the former is the increase in the difference between inner and outer values of the radial displacement; that is, a 3% difference in between the inner and outer radial displacement for the representative case becomes 30% and almost three times greater in the other two cases, respectively; examples of the latter are the different "distances" that the displacement profiles (each profile is plotted at a fixed time) are from each other (Figure 4.12, first column). Similar results concerning the degradation and Young's modulus profiles are observed, but the main feature is the qualitative changes in the nature of each solution. An almost homogeneous degradation in the thin-walled annulus becomes markedly inhomogeneous as the thickness increases. Degradation and consequent depreciation clearly proceed in the outward direction, as can be observed in the significant differences between degradation and the Young's modulus at the inner and outer surface (Figure 4.12, second and third columns).

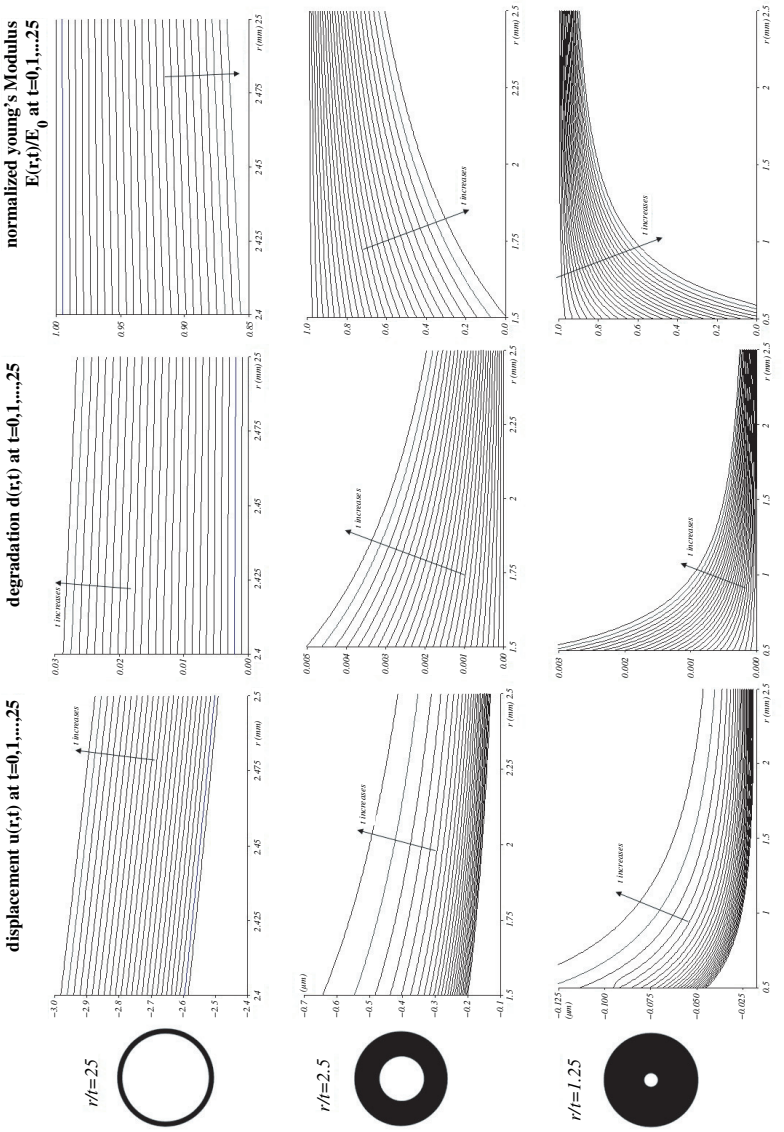

Figure 4.12. Influence of the wall thickness on the deformation, consequent degradation, and Young's modulus reduction. Profiles of displacement, degradation, and normalized Young's modulus for three different geometries are shown (the arrow means the increase in time). For a thin-walled cylinder such as a stent the degradation is almost homogeneous throughout the thickness. For the other two geometries, the inhomogeneity of the deformation is more intense. The inner and outer parts of the annulus are subjected to more different strain fields as the thickness increases and consequently greater asymmetries occur.

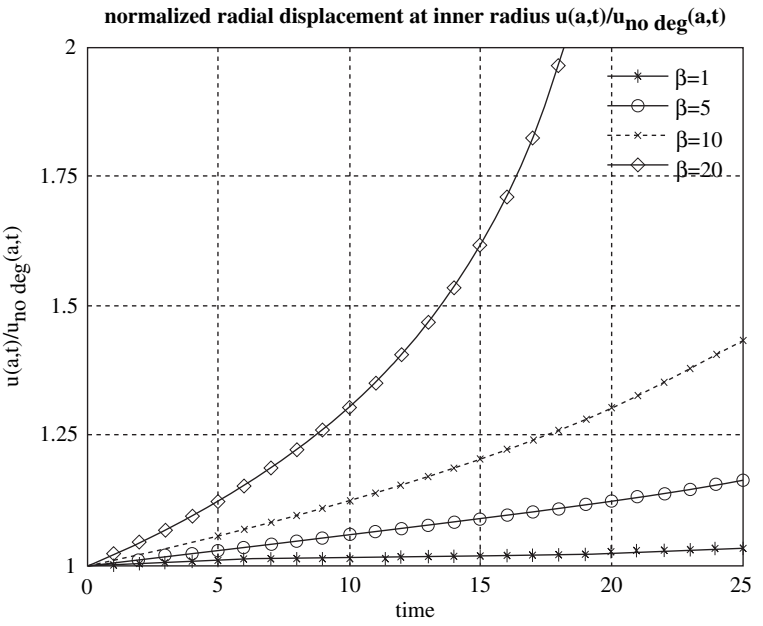

Figure 4.13. Normalized displacement at the inner radius $u(a,t)/unodeg(a,t)$ for several β. As β increases, the impact of degradation on the mechanical properties is greater. Although the outer pressure remains constant, the inner surface creeps inwards.

4.7.3 On the Role of the Constant Governing the Mechanical Properties Reduction, β

The main characteristic of the constant governing the Young's modulus reduction β is that when it increases in magnitude, so does the rate at which the material properties decrease due to a given degradation field (cf. Eq. (5.11)). Comparing several solutions with everything kept constant except the value of β, significant differences can be observed in the temporal evolution of the radial displacement, degradation, and Young's modulus at the inner surface (Figures 4.13, 4.14, and 4.15, respectively).

When $\beta = 20$ the annulus "collapses." This collapse is observed in all three figures: the displacement and degradation at the inner surface (the worst case scenario because the degradation proceeds from the inner surface) tend asymptotically to infinity whereas the Young's modulus reaches zero value. The numerical method does not converge, the computation is interrupted, and the assumption of classical elasticity does not hold anymore. On the other hand, a qualitative comparison between all the cases shown in the evolution of the Young's modulus profile (Figure 4.15) reveals

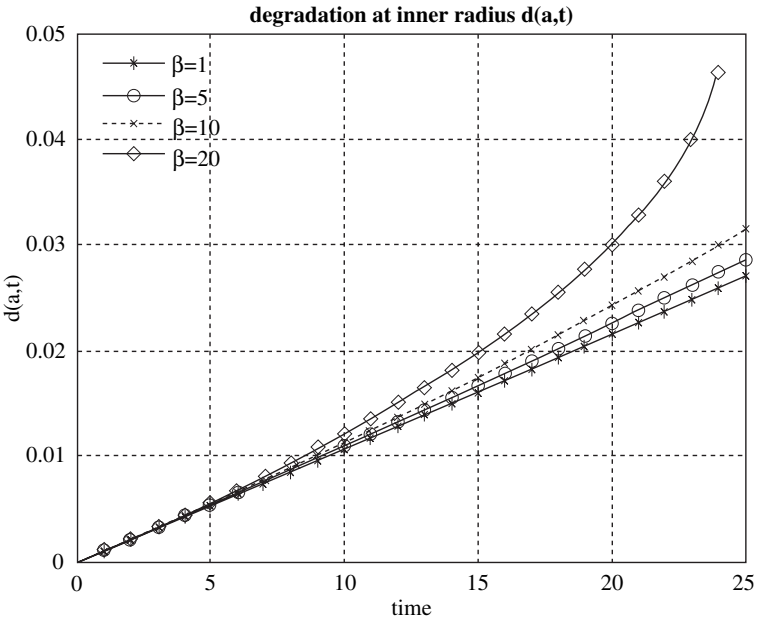

Figure 4.14. Degradation at the inner radius $d(a,t)$ for several β. The degradation increases asymptotically and ultimately will lead to the collapse.

that the impact in the mechanical properties and the likelihood of collapse is intimately related to the value of β. Lastly, β also influences the whole degradation process, as a softer material under the same load will be subjected to slightly greater strains and consequently to a slightly greater rate of degradation.

4.7.4 On the Parameter of the Mechanical Degradation Governing Equation, $D(t)$

The evolutions of the degradation at the inner surface for different $D(t)$ considered in the parametric study of the influence of the degradation parameter are clearly different from each other (Figure 4.16) and from the ones previously obtained in the parametric study for where the degradation achieved by each deformation is very close for all of the considered cases (cf. Figure 4.14). As $D(t)$ is connected to the amount of degradation that a given strain field can cause (cf. Eq. (5.13)), it follows logically that different values of this function will yield distinct degradations under the same strain field.

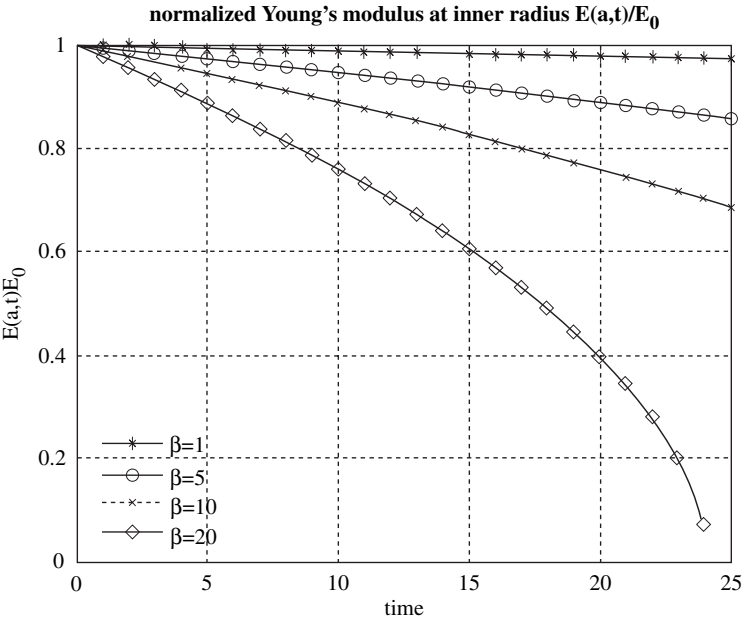

Figure 4.15. Normalized Young's modulus at the inner radius $E(a,t)/E_0$ for several β. As β increases, the ability to support load is readily depreciated by the degradation field. In the solution corresponding to $\beta = 20$, $E(a,t)$ tends to zero before $t = 25$ time units and is responsible for the blowing up of the approximating method.

Increasing the value of $D(t)$ intensifies the degradation that a given strain can provoke and therefore makes collapse more likely. Two cases collapse within the time march considered (Figures 4.17 and 4.18).

4.7.5 On the Shape of $D(t)$

When $D(t)$ is considered as shown in Figure 4.3, it is observed that $D(t) = 0$ leads to no degradation and this function can be used as an activation criterion for the initiation of strain-induced degradation. The annulus starts to yield as soon as the onset of degradation takes place (Figure 4.19). Because the absolute value of $D(t)$ is directly related to the amount of degradation imparted by a given strain field, the smoothness of the transient regime in the degradation evolution is a direct consequence of the smoothness of each $D(t)$. D4, with an abrupt change from 0 to 1 at $t = 20$, provokes an abrupt change in the degradation of the annulus; however, with D0, where the increase is linear over the first 20 time units, the transition is

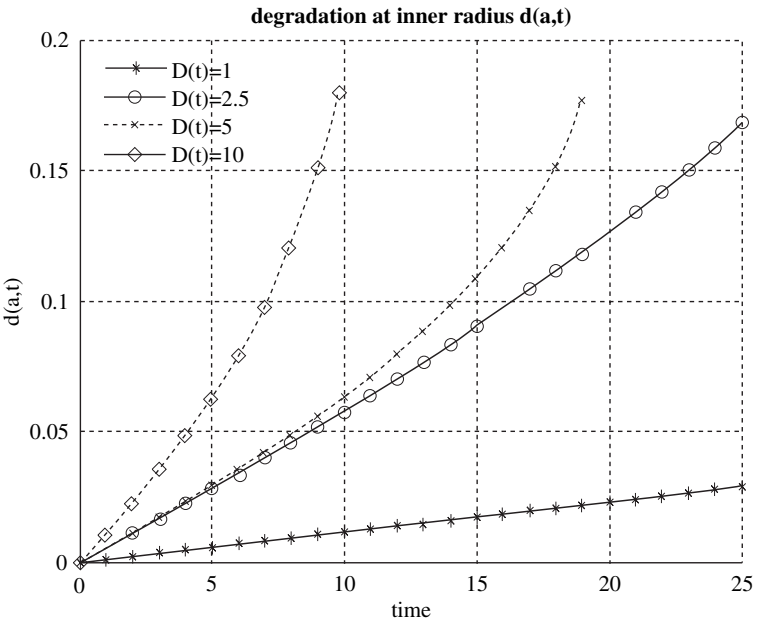

Figure 4.16. Degradation at inner radius $d(a,t)$ for several constant $D(t)$. Correspondingly, degradation increases at a faster rate for $D(t)$s of greater magnitude.

smoother (Figure 4.20). The functions tested ultimately end up with the value $D(t) = 1$ and it is observed that after a different transient period, degradation will eventually achieve approximately the same rate (slope in Figure 4.20), The time lag observed is a direct consequence of the different functions $D(t)$. Also, the annulus creeps inwards at an approximately constant rate and its material properties decrease in similar fashion for all the cases considered (slope in Figures 4.19 and 4.21).

4.8 Discussion

One particular case of the model for the mechanism of degradation shown in Figure 4.1 is the representative case taken as the initial result of the previous section. Data with the degradation parameters $\beta = 5$ and $D(t) = 1$ (cf. Figures 4.4 through 4.10), provide phenomenological support for the model. The annulus starts out nondegraded and the imposed loads in the inner and outer surfaces are responsible for a strain field through the balance

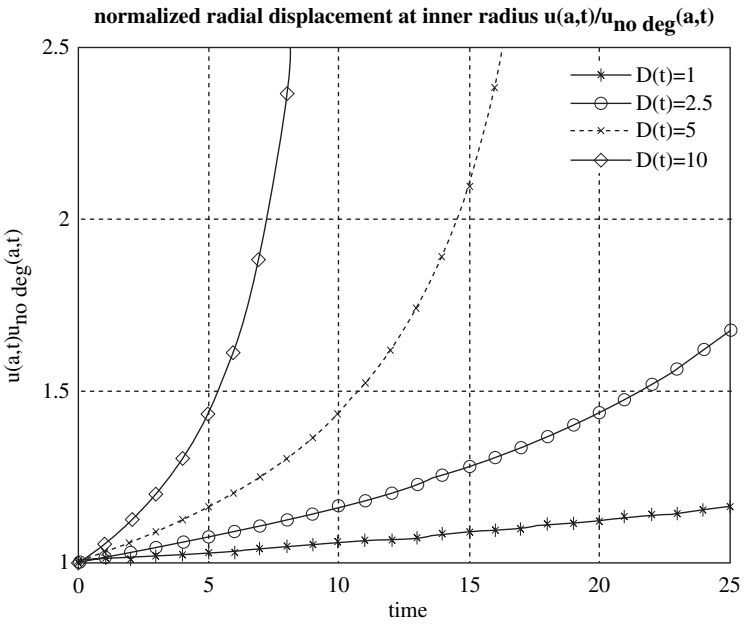

Figure 4.17. Normalized displacement at inner radius $u(a,t)/unodeg(a,t)$ for several $D(t)$. As the magnitude of $D(t)$ increases, the mechanical degradation induced by a strain field increases. Two cases ($D(t) = 5$ and $D(t) = 10$) reach the point of collapse in 25 time units.

of linear momentum (cf. Eq. (5.10)). Simultaneously, a degradation field dependent on the strain field given by the equation governing the increase of degradation (5.13) comes into play. Both are related by the classical constitutive equation (5.12), where the Young's modulus is assumed to depend on the degradation field.

The overall features of the solution obtained as the representative case clearly show an increase in the degradation field and a reduction in the mechanical properties (cf. Figures 4.5 and 4.6, respectively). A decrease of approximately 15% of the value of the non-degraded Young's modulus is seen over the time march considered. However, it must be remarked that such fast degradation is a consequence of this particular choice of the degradation parameters. The main purpose for this choice was to obtain quick degradation, so one would be able to observe its effects with a feasible time march. Also, because the time scales associated with degradation and a cycle of blood pressure considered in this model are of the same order of magnitude, one would observe the influence, if any, of an oscillating pressure applied on the inner surface. Lastly, it must be

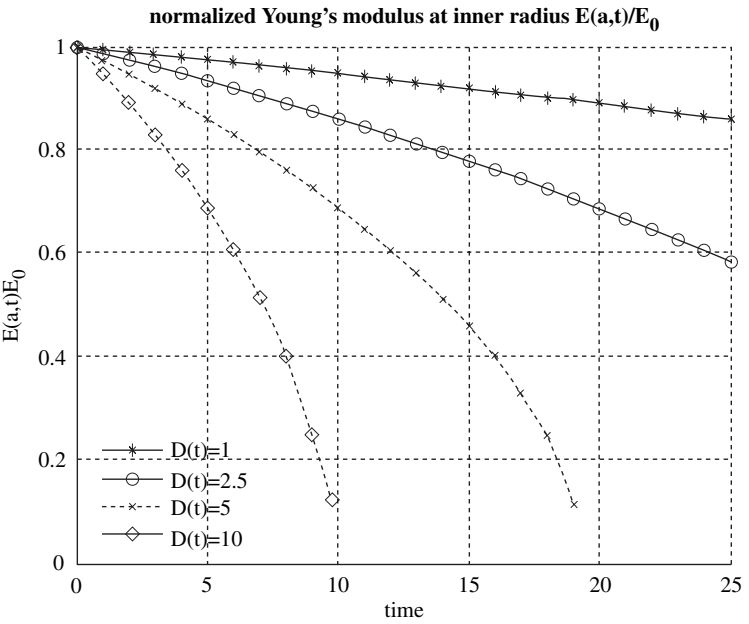

Figure 4.18. Normalized Young's modulus at inner radius $E(a,t)/E_0$ for several $D(t)$. A greater $D(t)$ would make a given strain yield a greater rate of increase of degradation.

remarked that in order to obtain a realistic model for describing a particular strain-degradable material, these parameters must be obtained from designed experiments.

The nonzero components of the stress tensor (Figures 4.8 through 4.10) have distinctive characteristics when compared with the nondegraded linear elastic case. The axial strain σ_{rr} is completely prescribed by the boundary conditions. Stress relaxation of the hoop stress $\sigma_{\theta\theta}$ is observed in the inner half of the annulus caused by local softening of the material. The strain field is higher in magnitude over the inner half and therefore degradation is greater over this region. Because the degraded cylindrical annulus must withstand the same loading conditions, the stresses in the outer part increase in magnitude to compensate for the softening and relaxation in the inner part. The axial strain shows a similar relaxation behavior, although less intense, deviating from the constancy through the thickness obtained in the standard case of a nondegradable elastic infinite cylinder.

Due to the same degradation mechanism, the cylinder creeps inwards under a constant load. The displacement progressively increases with time and that is a clear sign of creep (Figure 4.4). Under the same crushing load, the displacement of the inner surface increases due to degradation

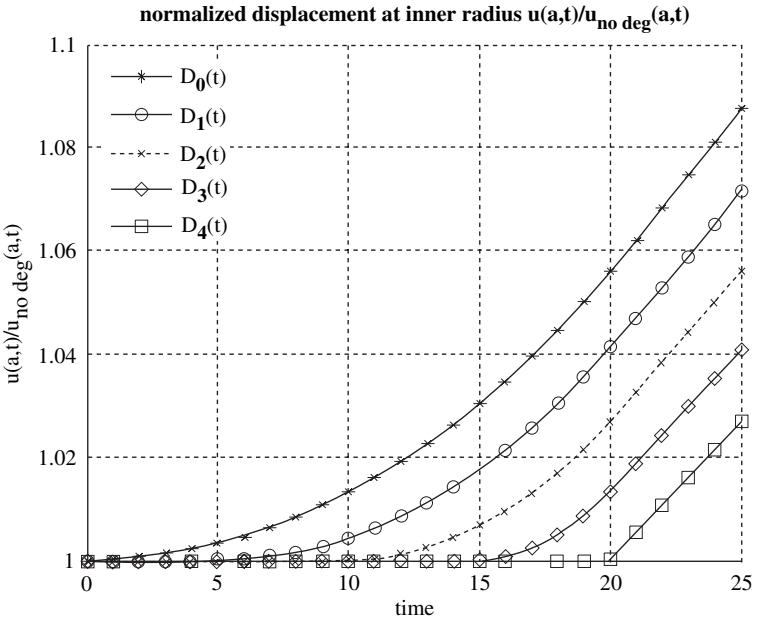

Figure 4.19. Normalized displacement at inner radius $u(a,t)/unodeg(a,t)$ for different functions $D(t)$. After a transient period, the cylinder creeps at an approximately constant rate.

and softening of the material. Thus the cylinder shrinks over time, inducing a higher strain field and consequently further degradation. On the other hand, when the evolution of the inner displacement is compared over time for different sets of degradation parameters (cf. Figures 4.13), it leads to such an intense degradation that the cylinder collapses inside the time march considered and the numerical scheme does not converge.

Also, the material shows behavior similar to mechanical hysteresis when the outer pressure is cycled between the inner pressure and its constant value. Hysteresis is obviously dependent on the degradation, as the two cases shown in Figure 4.11 demonstrate. As the degradation proceeds, the loading and unloading curves are far apart, meaning that dissipation increases over time and over degradation.

All these three distinct features are inherent characteristics of a viscoelastic material. However, strain-induced degradation of the material considered here shows similar characteristics. The material is elastic if no degradation occurs, but when degradation is active, the material shows stress relaxation, creep, and hysteresis, but markedly different from the similar phenomena exhibited by viscoelastic materials (cf. Rajagopal and Wineman for similar results on aging viscoelastic materials: two different

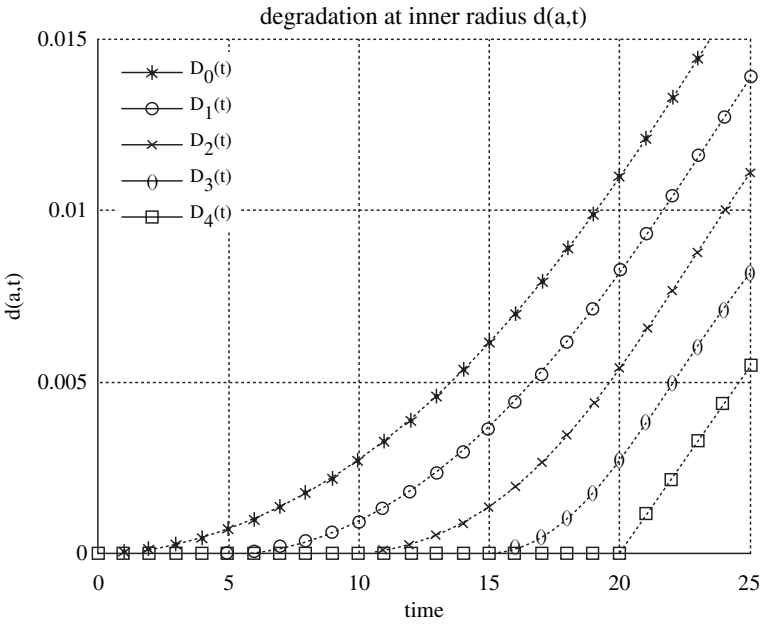

Figure 4.20. Degradation at inner radius $d(a,t)$ for different functions $D(t)$. The slope of each line will ultimately be the same and is related to the constant value that $D(t)$ assumes after $t = 20$.

components of the mechanisms of relaxation and creep were distinguished, one due to the inherent viscoelasticity of the material and the other due to aging processes [RAa]).

Another remarkable consequence of this degradation mechanism is its inhomogeneity. The equation governing degradation (5.13) states that degradation increases proportionally to the hoop strain. If two particles are subjected to different strains, consequently they will degrade to different extents. Their material properties, once the same before degradation, will vary with the current location. It is interesting how an initially homogeneous body becomes inhomogeneous after degradation induced by an inhomogeneous deformation.

Figure 4.12 shows qualitatively the differences among several inhomogeneous deformations. In the representative case, the profiles of displacement, degradation, and material properties reduction are almost straight lines. Each particle in the entire cross-section is subjected to an almost identical strain field and therefore the local degradation rates are similar and all particles of the body degrade approximately by the same amount. Thus, the differences in material properties are small. On the other hand, when the thickness of the cylinder is increased to obtain steeper hoop strain gradients

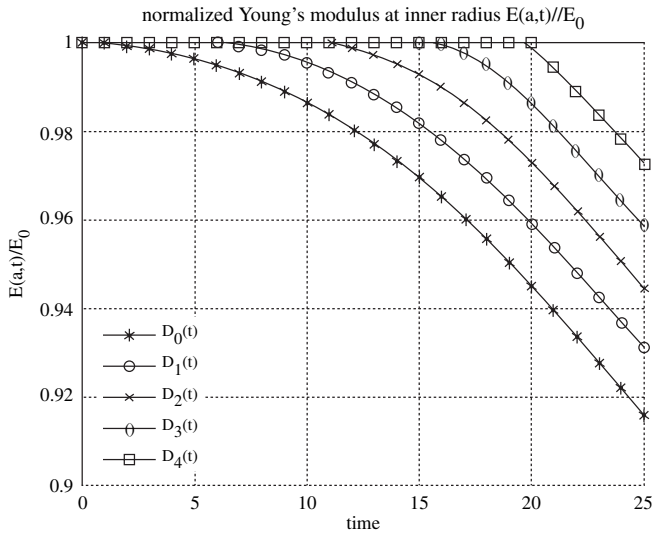

Figure 4.21. Normalized Young's modulus at inner radius $E(a,t)/E_0$ for different functions $D(t)$. The onset of degradation and consequent material properties reduction are directly related to $D(t)$ being nonzero.

throughout the thickness due to the inhomogeneity of the deformation, the degradation behavior of the body is completely different: (1) the flatness of the displacement profile is lost and the annulus is subjected to higher strains near the inside surface, (2) the degradation rate and the achieved degradation are greater in this region, (3) degradation clearly proceeds outwards, and (4) the differences in Young's modulus reduction obtained for different particles of the cylinder are enormous and the degree of inhomogeneity of the cylinder after some degradation is vast.

Degradation is driven by two distinct parameters that relate the two governing equations. Constant β appearing in the constitutive equation (5.12) through (5.11) represents the impact of a given amount of degradation in the reduction of the Young's modulus. This relationship can have a more general form (space- and time-dependence, nonlinear in the degradation field, or even dependent on the diffusion of certain species), and (5.11) is just one particular description of the impact of the degradation in the constitutive equation. In this simplified model, the relationship is linear and β is a constant (over space and time). The magnitude of β is ultimately related to the amount of depreciation that a given degradation would produce (a negative β would result in a material that strain hardens). Degradation is similar for the βs considered (Figure 4.14), but the corresponding Young's modulus reductions are clearly distinct (Figure 4.15).

The reason is that $D(t)$, which is responsible for the degradation due to a given strain field, is the same, whereas β changes dramatically, provoking different Young's modulus reductions for approximately the same degradation field. Eventually, because of the softening of the material, the cylinder yields and degrades progressively at slightly different rates. When $\beta = 20$, the effect of degradation in the Young's modulus is so strong that collapse was observed, that is, a point where the numerical solution yields a Young's modulus close to zero. It must be noted that all the solutions will eventually collapse after some time. The value of β, together with $D(t)$ will ultimately decide when collapse occurs.

$D(t)$ influences the process through the equation governing degradation (5.1) and (5.13). Equation (5.13) is a particular form of the more general (5.1). The parametric study of the effect of the absolute value of $D(t)$ yielded similar effects when compared with the influence of β (Figures 4.13 through 4.18). As expected, $D(t)$s of greater magnitude would motivate a stronger and faster degradation under the same strain field. Moreover, this parameter was chosen to be dependent on time in order to be possible to have activation criteria and temporal changes of the degradation rate. $D(t) = 0$ leads to no degradation and it can be used as an activation criterion (Figure 4.19). The rate of strain degradation will be closely related to this function. All five cases tend approximately to the same rate of degradation because all the $D(t)$s will ultimately have the value of 1. Young's modulus reduction and displacement at the inner surface show similar results (Figures 4.20 and 4.21).

As a final remark, it must be noted that this model is very simplistic in all its approximations: (1) a stent is not an infinite cylinder and this geometry was chosen in order to simplify the equations governing the process; (2) biodegradable polymers, such as PLLA, are not linear elastic materials and should be modeled as incompressible and fully nonlinear viscoelastic materials; (3) the particular forms of Eq. (5.13) and (5.11) describing the mechanism of degradation were chosen based on their simplicity, therefore the mechanism of strain-induced degradation is quite restrictive; and (4) mass balance must be met by taking ρ constant in the linear momentum balance (5.9); thus this model describes the initial steps of the overall process when degradation occurs without significant effects of erosion or elimination.

4.9 Conclusions

As a first step towards a fully nonlinear model, biodegradable polymers were modeled as a class of linearized materials. From the phenomenological

acceptable results obtained with this model, one concludes that strain-induced degradation can be modeled with a partial differential equation governing the rate of increase of degradation coupled with the equations of motion. The constitutive equation takes into account the effect of degradation of the mechanical properties.

The material with degradation considered here shows stress relaxation, creep, and hysteresis, thus a dissipative process governing this particular degradation mechanism. Inhomogeneous deformations lead to inhomogeneous degradations, hence the homogeneous cylinder considered here becomes inhomogeneous after the onset of degradation.

The efficacy of this approach was verified by solving this simple problem and the constitutive model will be integrated into a finite element software package in order to analyze more realistic and more complex stent geometries. Later, the model will be extended in such a way that it will be capable of describing the diffusion of a drug impregnated in the material reflecting the enhancement of the diffusion due to changes in the porosity due to degradation.

Acknowledgments

This work was partially funded by the Portuguese FCT - Fundação para a Ciência e Tecnologia (SFRH/BD/17060/2004) and NIH grant R01 EB000115. A general thermodynamic framework for bodies capable of undergoing strain-induced degradation is being developed and will be published.

4.10 References

[AGa] Agrawal, C.M., and Clark, H.G., Deformation characteristics of a bioabsorbable intravascular stent. *Invest. Radiol.*, **27** (1992), 1020–4.

[AGb] Agrawal, C.M., Haas, K.F., Leopold, D.A., and Clark, H.G., Evaluation of poly(L-lactic acid) as a material for intravascular polymeric stents. *Biomaterials*, **13** (1992), 176–82.

[AHa] Ahn, Y.K., Jeong, M.H., Kim, J.W., et al., Preventive effects of the heparin-coated stent on restenosis in the porcine model. *Catheter Cardiovasc. Interv.*, **48** (1999), 324–30.

[ALa] Al Suwaidi, J., Berger, P.B., and Holmes, D.R., Jr., Coronary artery stents. *JAMA*, **284** (2000), 1828–36.

[ALb] Ali, S.A., Doherty, P.J., and Williams, D.F., Mechanisms of polymer degradation in implantable devices. 2. Poly(DL-lactic acid). *J. Biomed. Mater. Res.*, **27** (1993), 1409–18.

[ALc] Ali, S.A., Zhong, S.P., Doherty, P.J., and Williams, D.F., Mechanisms of polymer degradation in implantable devices. 1. Poly (caprolactone). *Biomaterials*, **14** (1993), 648–56.

[ARa] Ardissino, D., Cavallini, C., Bramucci, E., et al., Sirolimus-eluting vs. uncoated stents for prevention of restenosis in small coronary arteries: a randomized trial, *JAMA*, **292** (2004), 2727–34.

[ATa] Athanasiou, K.A., Agrawal, C.M., Barber, F.A., and Burkhart, S.S., Orthopaedic applications for PLA-PGA biodegradable polymers. *Arthroscopy J. Arthroscopic Related Surg.*, **14** (1998), 726–37.

[AXa] Axel, D.I., Kunert, W., Goggelmann, C., et al., Paclitaxel inhibits arterial smooth muscle cell proliferation and migration in vitro and in vivo using local drug delivery. *Circulation*, **96** (1997), 636–45.

[BAa] Babapulle, M.N., and Eisenberg, M.J., Coated stents for the prevention of restenosis: Part II. *Circulation*, **106** (2002), 2859–66.

[BEa] Bedoya, J., Meyer, C.A., Timmins, L.H., Moreno, M.R., and Moore, J.E., Jr., Effects of stent design parameters on artery wall mechanics (submitted).

[BEb] Bellenger, V., Ganem, M., Mortaigne, B., and Verdu, J., Lifetime prediction in the hydrolytic aging of polyesters. *Polym. Degradation Stability*, **49** (1995), 91–7.

[BEc] Bertrand, O.F., Sipehia, R., Mongrain, R., et al., Biocompatibility aspects of new stent technology. *J. Am. Coll. Cardiol.*, **32** (1998), 562–71.

[BIa] Bier, J.D., Zalesky, P., Li, S.T., Sasken, H., and Williams, D.O., A new bioabsorbable intravascular stent: in vitro assessment of hemodynamic and morphometric characteristics. *J. Interv. Cardiol.*, **5** (1992), 187–94.

[BLa] Blindt, R., Hoffmeister, K.M., Bienert, H., et al., Development of a new biodegradable intravascular polymer stent with simultaneous incorporation of bioactive substances. *Int. J. Artif. Organs*, **22** (1999), 843–53.

[BOa] Bose, S.M., and Git, Y., Mathematical modelling and computer simulation of linear polymer degradation: Simple scissions. *Macromol. Theor. Simul.*, **13** (2004), 453–73.

[BRa] Browarzik, D., and Koch, A., Application of continuous kinetics to polymer degradation. *J. Macromol. Sci. Pure Appl. Chem.*, **33A** (1996), 1633–41.

[BUa] Burkersroda, F.v., Schedl, L., and Gopferich, A., Why degradable polymers undergo surface erosion or bulk erosion. *Biomaterials*, **23** (2002), 4221–31.

[COa] Colombo, A., and Karvouni, E., Biodegradable stents : "Fulfilling the mission and stepping away." *Circulation*, **102** (2000), 371–3.

[CUa] Currier, J.W., and Faxon, D.P., Restenosis after percutaneous transluminal coronary angioplasty: have we been aiming at the wrong target? *J. Am. Coll. Cardiol.*, **25** (1995), 516–20.

[DEa] De Scheerder, I.K., Wilczek, K.L., Verbeken, E.V., et al., Biocompatibility of biodegradable and nonbiodegradable polymer-coated stents implanted in porcine peripheral arteries. *Cardiovasc. Intervent. Radiol.*, **18** (1995), 227–32.

[DEb] De Scheerder, I.K., Wilczek, K.L., Verbeken, E.V., et al., Biocompatibility of polymer-coated oversized metallic stents implanted in normal porcine coronary arteries. *Atherosclerosis*, **114** (1995), 105–14.

[DEc] DePalma, V.A., Baier, R.E., Ford, J.W., Glott, V.L., and Furuse, A., Investigation of three-surface properties of several metals and their relation to blood compatibility. *J. Biomed. Mater. Res.*, **6** (1972), 37–75.

[DIa] Di Mario, C., Griffiths, H., Goktekin, O., et al., Drug-eluting bioabsorbable magnesium stent. *J. Interv. Cardiol.*, **17** (2004), 391–5.

[DOa] Dotter, C.T., Transluminal angioplasty: A long view. *Radiology*, **135** (1980), 561–4.

[DOb] Douglas, J.S., Jr., King, S.B., 3rd, and Roubin, G.S., Influence of the methodology of percutaneous transluminal coronary angioplasty on restenosis. *Am. J. Cardiol.*, **60** (1987), 29B–33B.

[DRa] Drumright, R.E., Gruber, P.R., and Henton, D.E., Polylactic acid technology. *Adv. Mater.*, **12** (2000), 1841–6.

[DUa] Duda, S.H., Bosiers, M., Lammer, J., et al., Sirolimus-eluting versus bare nitinol stent for obstructive superficial femoral artery disease: The SIROCCO II trial. *J. Vasc. Interv. Radiol.*, **16** (2005), 331–8.

[DUb] Duda, S.H., Pusich, B., Richter, G., et al., Sirolimus-eluting stents for the treatment of obstructive superficial femoral artery disease: Six-month results. *Circulation*, **106** (2002), 1505–9.

[EDa] Edelman, E.R., and Rogers, C., Pathobiologic responses to stenting. *Am. J. Cardiol.*, **81** (1998), 4E–6E.

[FAa] Farb, A., Weber, D.K., Kolodgie, F.D., Burke, A.P., and Virmani, R., Morphological predictors of restenosis after coronary stenting in humans. *Circulation*, **105** (2002), 2974–80.

[FAb] Faxon, D.P., Vascular stents. *Rev. Cardiovasc. Med.*, **2** (2001), 106–7.

[FIa] Fischell, TA., Polymer coatings for stents. Can we judge a stent by its cover? *Circulation*, **94** (1996), 1494–5.

[FIb] Fischman, D.L., Leon, M.B., Baim, D.S., et al., A randomized comparison of coronary-stent placement and balloon angioplasty in the treatment of coronary-artery disease. *N. Engl. J. Med.*, **331** (1994), 496–501.

[GAa] Gallo, R., Padurean, A., Jayaraman, T., et al., Inhibition of intimal thickening after balloon angioplasty in porcine coronary arteries by targeting regulators of the cell cycle. *Circulation*, **99** (1999), 2164–70.

[GAb] Garlotta, D., A literature review of poly(lactic acid). *J. Polym. Environ.*, **9** (2001), 63–84.

[GLa] Glagov, S., Zarins, C.K., Masawa, N., Xu, CP., Bassiouny, H., and Giddens, D.P., Mechanical functional role of non-atherosclerotic intimal thickening. *Front. Med. Biol. Eng.*, **5** (1993), 37–43.

[GLb] Glagov, S., Intimal hyperplasia, vascular modeling, and the restenosis problem. *Circulation*, **89** (1994), 2888–91.

[GOa] Gopferich, A., and Langer, R., Modeling polymer erosion. *Macromolecules*, **26** (1993), 4105–12.

[GOb] Gopferich, A., Mechanisms of polymer degradation and elimination. In: Domb, A.J., Kost, J., and Wiseman, D.M., Eds. **Handbook of Biodegradable Polymers**. Harwood Academic, Australia (1997), 451–71.

[GOc] Gopferich, A., Polymer degradation and erosion: Mechanisms and applications. *Eur. J. Pharm. Biopharm.*, **4** (1996), 1–11.

[GRa] Grabow, N., Martin, H., and Schmitz, K.P., The impact of material characteristics on the mechanical properties of a poly(L-lactide) coronary stent. *Biomed. Tech. (Berl.)*, **47** (2002), 503–5.

[GRb] Grabow, N., Schlun, M., Sternberg, K., Hakansson, N., Kramer, S., and Schmitz, K.P., Mechanical properties of laser cut poly(L-lactide) micro-specimens: Implications for stent design, manufacture, and sterilization. *J. Biomech. Eng.*, **127** (2005), 25–31.

[GRc] Grube, E., Gerckens, U., Muller, R., and Bullesfeld, L., Drug eluting stents: Initial experiences. *Z. Kardiol.*, **91** (2002), 44–8.

[GRd] Grube, E., Silber, S., Hauptmann, K.E., et al., TAXUS I: Six- and twelve-month results from a randomized, double-blind trial on a slow-release paclitaxel-eluting stent for de novo coronary lesions. *Circulation*, **107** (2003), 38–42.

[GUa] Gutwald, R., Pistner, H., Reuther, J., and Muhling, J., Biodegradation and tissue-reaction in a long-term implantation study of poly (L-Lactide). *J. Mater. Sci. Mater. Med.*, **5** (1994), 485–90.

[HAa] Hawkins, W.L., Polymer degradation. In: Polymer degradation and stabilization. Springer-Verlag, Berlin (1984) 3–34.

[HAb] Hayashi, T., Biodegradable polymers for biomedical uses. *Prog. Polym. Sci.*, **19** (1994), 663–702.

[HEa] Heublein, B., Rohde, R., Kaese, V., Niemeyer, M., Hartung W., and Haverich, A., Biocorrosion of magnesium alloys: A new principle in cardiovascular implant technology? *Heart*, **89** (2003), 651–6.

[HIa] Hietala, E.M., Salminen, U.S., Stahls, A., et al., Biodegradation of the copolymeric polylactide stent. Long-term follow-up in a rabbit aorta model. *J. Vasc. Res.*, **38** (2001), 361–9.

[HOa] Holmes, D.R., Camrud, A.R., Jorgenson, M.A., Edwards, W.D., and Schwartz, R.S., Polymeric stenting in the porcine coronary artery model: Differential outcome of exogenous fibrin sleeves versus polyurethane-coated stents. *J. Am. Coll. Cardiol.*, **24** (1994), 525–31.

[HYa] Hyon, S.H., Jamshidi, K., and Ikada, Y., Effects of residual monomer on the degradation of DL-lactide polymer. *Polym. Int.*, **46** (1998), 196–202.

[ISa] Isotalo, T., Talja, M., Valimaa, T., Tormala, P., and Tammela, T.L., A bioabsorbable self-expandable, self-reinforced poly-L-lactic acid urethral stent for recurrent urethral strictures: Long-term results. *J. Endourol.*, **16** (2002), 759–62.

[IVa] Ivanova, T., Grozev, N., Panaiotov, I., and Proust, J.E., Role of the molecular weight and the composition on the hydrolysis kinetics of monolayers of poly(alpha-hydroxy acid)s. *Colloid Polym. Sci.*, **277** (1999), 709–18.

[JEa] Jeremias, A., Sylvia, B., Bridges, J., et al., Stent thrombosis after successful sirolimus-eluting stent implantation. *Circulation*, **109** (2004), 1930–2.

[JOa] Joshi, A., and Himmelstein, K.J., Dynamics of controlled release from bioerodible matrices. *J. Control. Release*, **15** (1991), 95–104.

[KAa] Kastrati, A., Dibra, A., Eberle, S., et al., Sirolimus-eluting stents vs. paclitaxel-eluting stents in patients with coronary artery disease: meta-analysis of randomized trials. *JAMA*, **294** (2005), 819–25.

[KAb] Kastrati, A., Hall, D., and Schomig, A., Long-term outcome after coronary stenting. *Curr. Control Trials Cardiovasc. Med.*, **1** (2000), 48–54.

[KAc] Katti, D.S., Lakshmi, S., Langer, R., and Laurencin, C.T., Toxicity, biodegradation and elimination of polyanhydrides. *Adv. Drug Deliv. Rev.*, **54** (2002), 933–61.

[KHa] Khang, G., Rhee, J.M., Jeong, J.K., et al., Local drug delivery system using biodegradable polymers. *Macromol. Res.*, **11** (2003), 207–23.

[KIa] Kimura, T., Yokoi, H., Nakagawa, Y., et al., Three-year follow-up after implantation of metallic coronary-artery stents. *N. Engl. J. Med.*, **334** (1996), 561–6.

[LAa] Labinaz, M., Zidar, J.P., Stack, R.S., and Phillips, H.R., Biodegradable stents: The future of interventional cardiology? *J. Interv. Cardiol.*, **8** (1995), 395–405.

[LAb] Lambert, T.L., Dev, V., Rechavia, E., Forrester, J.S., Litvack F, and Eigler, N.L., Localized arterial wall drug delivery from a polymer-coated removable metallic stent. Kinetics, distribution, and bioactivity of forskolin. *Circulation*, **90** (1994), 1003–11.

[LAc] Langer, R., Drug delivery and targeting. *Nature*, **392** (1998), 5–10.

[LAd] Laufman, H., and Rubel, T., Synthetic absorbable sutures. *Surg. Gynecol. Obstet.*, **145** (1977), 597–608.

[LEa] Lemos, P.A., Serruys, P.W., van Domburg, R.T., et al., Unrestricted utilization of sirolimus-eluting stents compared with conventional bare stent implantation in the "real world": The Rapamycin-eluting stent evaluated at Rotterdam Cardiology Hospital (RESEARCH) registry. *Circulation*, **109** (2004), 190–5.

[LEb] Levenberg, S., and Langer, R., Advances in tissue engineering. In: **Current Topics in Developmental Biology**, Vol 61. Elsevier, San Diego (2004) 113.

[LIa] Li, S.M., and McCarthy, S., Further investigations on the hydrolytic degradation of poly(DL-lactide). *Biomaterials*, **20** (1999), 35–44.

[LIb] Li, S.M., and Vert, M., Morphological-Changes Resulting from the hydrolytic degradation of stereocopolymers derived from L-lactides and Dl-lactides. *Macromolecules*, **27** (1994), 3107–10.

[LIc] Libby, P., Schwartz, D., Brogi, E., Tanaka, H., and Clinton, S.K., A cascade model for restenosis. A special case of atherosclerosis progression. *Circulation*, **86** (1992), 11147–52.

[LId] Lincoff, A.M., Furst, J.G., Ellis, S.G., Tuch, R.J., and Topol, E.J., Sustained local delivery of dexamethasone by a novel intravascular eluting stent to prevent restenosis in the porcine coronary injury model. *J. Am. Coll. Cardiol.*, **29** (1997), 808–16.

[LIe] Lincoff, A.M., Topol, E.J., and Ellis, S.G., Local drug delivery for the prevention of restenosis. Fact, fancy, and future. *Circulation*, **90** (1994), 2070–84.

[LIf] Lipinski, M.J., Fearon, W.F., Froelicher, V.F., and Vetrovec, G.W., The current and future role of percutaneous coronary intervention in patients with coronary artery disease. *J. Interv. Cardiol.*, **17** (2004), 283–94.

[LUa] Lunt, J., Large-scale production, properties and commercial applications of polylactic acid polymers. *Polym. Degradation Stability*, **59** (1998), 145–52.

[MAa] Marx, S.O., Jayaraman, T., Go, L.O., and Marks, A.R., Rapamycin-Fkbp inhibits cell-cycle regulators of proliferation in vascular smooth-muscle cells. *Circulation Res.*, **76** (1995), 412–7.

[MIa] Middleton, J.C., and Tipton, A.J., Synthetic biodegradable polymers as orthopedic devices. *Biomaterials*, **21** (2000), 2335–46.

[MIb] Mintz, G.S., Hoffmann, R., Mehran, R., et al., In-stent restenosis: The Washington Hospital Center experience. *Am. J. Cardiol.*, **81** (1998), 7E–13E.

[MIc] Mintz, G.S., Popma, J.J., Pichard, A.D., et al., Arterial remodeling after coronary angioplasty: A serial intravascular ultrasound study. *Circulation*, **94** (1996), 35–43.

[MOa] Moore, J., Jr., and Berry, J.L., Fluid and solid mechanical implications of vascular stenting. *Ann. Biomed. Eng.*, **30** (2002), 498–508.

[MOb] Morice, M.C., Serruys, P.W., Sousa, J.E., et al., A randomized comparison of a sirolimus-eluting stent with a standard stent for coronary revascularization. *N. Engl. J. Med.*, **346** (2002), 1773–80.

[Moc] Moses, J.W., Leon, M.B., Popma, J.J., et al., Sirolimus-eluting stents versus standard stents in patients with stenosis in a native coronary artery. *N. Engl. J. Med.*, **349** (2003), 1315–23.

[MUa] Muller, D.W., Ellis, S.G., and Topol, E.J., Experimental models of coronary artery restenosis. *J. Am. Coll. Cardiol.*, **19** (1992), 418–32.

[MUb] Murphy, J.G., Schwartz, R.S., Edwards, W.D., Camrud, A.R., Vlietstra RE, and Holmes, D.R., Jr. Percutaneous polymeric stents in porcine coronary arteries. Initial experience with polyethylene terephthalate stents. *Circulation*, **86** (1992), 1596–604.

[MUc] Murphy, J.G., Schwartz, R.S., Huber, K.C., and Holmes, D.R., Jr. Polymeric stents: Modern alchemy or the future? *J. Invasive. Cardiol.*, **3** (1991), 144–8.

[NGa] Nguyen, K.T., Su, S.H., Sheng, A., et al., In vitro hemocompatibility studies of drug-loaded poly-(L-lactic acid) fibers. *Biomaterials*, **24** (2003), 5191–201.

[NGb] Nguyen, T.Q., and Kausch, H.H., GPC data interpretation in mechanochemical polymer degradation. *Int. J. Polym. Anal. Characterization*, **4** (1998), 447–70.

[NGc] Nguyen, T.Q., Kinetics of mechanochemical degradation by gel permeation chromatography. *Polym. Degradation Stability*, **46** (1994), 99–111.

[NUa] Nuutinen, J.P., Clerc, C., and Tormala, P., Theoretical and experimental evaluation of the radial force of self-expanding braided bioabsorbable stents. *J. Biomater. Sci. Polym. Ed.*, **14** (2003), 677–87.

[ONa] Ong, A.T., Serruys, P.W., and Aoki, J., et al., The unrestricted use of paclitaxel- versus sirolimus-eluting stents for coronary artery disease in an unselected population: One-year results of the Taxus-Stent Evaluated at Rotterdam Cardiology Hospital (T-SEARCH) registry. *J. Am. Coll. Cardiol.*, **45** (2005), 1135–41.

[OTa] Ottenbrite, R.M., Albertsson, and A.C., Scott, G., Discussion on degradation terminology. In: Vert, M., Feijen, J., Albertsson, A.C., Scott, G., Chiellini, E., Eds. **Biodegradable Polymers and Plastics**. The Royal Society of Chemisty, Cambridge (1992) 73–92.

[PAa] Palmaz, J.C., Balloon-expandable intravascular stent. *AJR Am. J. Roentgenol.*, **150** (1988), 1263–9.

[PEa] Peng, T., Gibula, P., Yao K.-d., and Goosen, M.F.A., Role of polymers in improving the results of stenting in coronary arteries. *Biomaterials*, **17** (1996), 685–94.

[PEb] Peuster, M., Wohlsein, P., Brugmann, M., et al., A novel approach to temporary stenting: Degradable cardiovascular stents produced from corrodible metal-results 6-18 months after implantation into New Zealand white rabbits. *Heart*, **86** (2001), 563–9.

[PIa] Pietrzak, W.S., Sarver, D.R., and Verstynen, M.L., Bioabsorbable polymer science for the practicing surgeon. *J. Craniofac. Surg.*, **8** (1997), 87–91.

[PIb] Pietrzak, W.S., Verstynen, M.L., and Sarver, D.R., Bioabsorbable fixation devices: Status for the craniomaxillofacial surgeon. *J. Craniofac. Surg.*, **8** (1997), 92–6.

[PIc] Pistner, H., Bendix, D.R., Muhling, J., and Reuther, J.F., Poly (L-Lactide) — A long-term degradation study invivo .3. Analytical characterization. *Biomaterials*, **14** (1993), 291–8.

[PId] Pistner, H., Gutwald, R., Ordung, R., Reuther, J., and Muhling, J., Poly(L-lactide) — A long-term degradation study in-vivo.1. Biological results. *Biomaterials*, **14** (1993), 671–7.

[RAa] Rajagopal, K.R., and Wineman, A.S., A note on viscoelastic materials that can age. *Int. J. NonLinear Mech.*, **39** (2004), 1547–54.

[ROa] Robaina, S., Jayachandran, B., He, Y., et al., Platelet adhesion to simulated stented surfaces. *J. Endovasc. Ther.*, **10** (2003), 978–86.

[ROb] Rogers, C., and Edelman, E.R., Endovascular stent design dictates experimental restenosis and thrombosis. *Circulation*, **91** (1995), 2995–3001.

[ROc] Roubin, G.S., Douglas, J.S., Jr., King, S.B., 3rd, et al., Influence of balloon size on initial success, acute complications, and restenosis after percutaneous transluminal coronary angioplasty. A prospective randomized study. *Circulation*, **78** (1988), 557–65.

[SAa] Saia, F., Marzocchi, A., and Serruys, P.W., Drug-eluting stents. The third revolution in percutaneous coronary intervention. *Ital. Heart J.*, **6** (2005), 289–303.

[SAb] Sarembock, I.J., LaVeau, P.J., Sigal, S.L., et al., Influence of inflation pressure and balloon size on the development of intimal hyperplasia after balloon angioplasty. A study in the atherosclerotic rabbit. *Circulation*, **80** (1989), 1029–40.

[SCa] Schakenraad, J.M., Hardonk, M.J., Feijen, J., Molenaar, I., and Nieuwenhuis, P., Enzymatic activity toward poly(L-lactic acid) implants. *J. Biomed. Mater. Res.*, **24** (1990), 529–45.

[SCb] Schatz, R.A., Baim, D.S., Leon, M., et al., Clinical-experience with the Palmaz-Schatz coronary stent - Initial results of a multicenter study. *Circulation*, **83** (1991), 148–61.

[SCc] Schatz, R.A., Introduction to intravascular stents. *Cardiol. Clin.*, **6** (1988), 357–72.

[SCd] Schnabel, W., **Polymer Degradation**. Macmillan, New York (1981).

[SCe] Schofer, J., Schluter, M., Gershlick, A.H., et al., Sirolimus-eluting stents for treatment of patients with long atherosclerotic lesions in small coronary arteries: Double-blind, randomised controlled trial (E-SIRIUS). *Lancet*, **362** (2003), 1093–9.

[SCf] Schwartz, R.S., Neointima and arterial injury: Dogs, rats, pigs, and more. *Lab. Invest.*, **71** (1994), 789–91.

[SCg] Schwartz, R.S., Pathophysiology of restenosis: Interaction of thrombosis, hyperplasia, and/or remodeling. *Am. J. Cardiol.*, **81** (1998), 14E–7E.

[SEa] Serruys, P.W., Dejaegere, P., Kiemeneij, F., et al., A comparison of balloon-expandable-stent implantation with balloon angioplasty in patients with coronary-artery disease. *N. Engl. J. Med.*, **331** (1994), 489–95.

[SEb] Serruys, P.W., Emanuelsson, H., van der Giessen, W., et al., Heparin-coated Palmaz–Schatz stents in human coronary arteries. Early outcome of the Benestent-II Pilot Study. *Circulation*, **93** (1996), 412–22.

[SIa] Siepmann, J., and Gopferich, A., Mathematical modeling of bioerodible, polymeric drug delivery systems. *Adv. Drug Delivery Rev.*, **48** (2001), 229–47.

[SIb] Sigwart, U., Puel, J., Mirkovitch, V., Joffre, F., and Kappenberger, L., Intravascular stents to prevent occlusion and restenosis after transluminal angioplasty. *N. Engl. J. Med.*, **316** (1987), 701–6.

[SIc] Silber, S., Hamburger, J., Grube, E., et al., Direct stenting with TAXUS stents seems to be as safe and effective as with predilatation. A post hoc analysis of TAXUS II. *Herz*, **29** (2004), 171–80.

[SId] Siparsky, G.L., Voorhees, K.J., and Miao, F.D., Hydrolysis of polylactic acid (PLA) and polycaprolactone (PCL) in aqueous acetonitrile solutions: Autocatalysis. *J. Environ. Polym. Degradation*, **6** (1998), 31–41.

[STa] Staab, M.E., Holmes, D.R., and Schwartz, R.S., Polymers. In: Sigwart U, Ed. **Endoluminal Stenting**. WB Saunders, London (1996), 34–44.

[STb] Stone, G.W., Ellis, S.G., Cox, D.A., et al., One-year clinical results with the slow-release, polymer-based, paclitaxel-eluting TAXUS stent: The TAXUS-IV trial. *Circulation*, **109** (2004), 1942–7.

[SUa] Su, S.H., Chao, R.Y., Landau, C.L., et al., Expandable bioresorbable endovascular stent. I. Fabrication and properties. *Ann. Biomed. Eng.*, **31** (2003), 667–77.

[TAa] Tamada, J.A., and Langer, R., Erosion kinetics of hydrolytically degradable polymers. *Proceedings of the National Academy of Sciences of the United States of America*, **90** (1993), 552–6.

[TAb] Tamai, H., Igaki, K., Kyo, E., et al., Initial and 6-month results of biodegradable poly-l-lactic acid coronary stents in humans. *Circulation*, **102** (2000), 399–404.

[TAc] Tamai, H., Igaki, K., Tsuji, T., et al., A biodegradable poly-L-lactic acid coronary stent in the porcine coronary artery. *J. Interven. Cardiol.*, **12** (1999), 443–9.

[TAd] Tammela, T.L., and Talja, M., Biodegradable urethral stents. *BJU Int.*, **92** (2003), 843–50.

[TAe] Tanabe, K., Serruys, P.W., Grube, E., et al., TAXUS III Trial: In-stent restenosis treated with stent-based delivery of paclitaxel incorporated in a slow-release polymer formulation. *Circulation*, **107** (2003), 559–64.

[THa] Therasse, E., Soulez, G., Cartier, P., et al., Infection with fatal outcome after endovascular metallic stent placement. *Radiology*, **192** (1994), 363–5.

[THb] Thombre, A.G., Theoretical aspects of polymer biodegradation: Mathematical modeling of drug release and acid-catalyzed poly(othoester) biodegradation. In: Vert, M., Feijen, J., Albertsson, A.C., Scott, G., Chiellini, E., Eds. **Biodegradable Polymers and Plastics**. The Royal Society of Chemisty, Cambridge (1992) 214–25.

[TSa] Tsuji, T., Tamai, H., Igaki, K., et al., Biodegradable polymeric stents. *Curr. Interv. Cardiol. Rep.*, **3** (2001), 10–7.

[TSb] Tsuji, T., Tamai, H., Igaki, K., et al., Biodegradable stents as a platform to drug loading. *Int. J. Cardiovasc. Intervent.*, **5** (2003), 13–6.

[UNa] Unverdorben, M., Spielberger, A., Schywalsky, M., et al., A polyhydroxybutyrate biodegradable stent: Preliminary experience in the rabbit. *Cardiovasc. Intervent. Radiol.*, **25** (2002), 127–32.

[UUa] Uurto, I., Mikkonen, J., Parkkinen, J., et al., Drug-eluting biodegradable poly-D/L-lactic acid vascular stents: An experimental pilot study. *J. Endovasc. Ther.*, **12** (2005), 371–9.

[VAa] Valimaa, T., Laaksovirta, S., Tammela, T.L., et al., Viscoelastic memory and self-expansion of self-reinforced bioabsorbable stents. *Biomaterials*, **23** (2002), 3575–82.

[VAb] van der Giessen, W.J., Lincoff, A.M., Schwartz, R.S., et al., Marked inflammatory sequelae to implantation of biodegradable and nonbiodegradable polymers in porcine coronary arteries. *Circulation*, **94** (1996), 1690–7.

[VAc] van der Giessen, W.J., Slager, C.J., Gussenhoven, E.J., et al., Mechanical features and in vivo imaging of a polymer stent. *Int. J. Card. Imaging.*, **9** (1993), 219–26.

[VAd] van der Giessen, W.J., Slager, C.J., van Beusekom, H.M., et al., Development of a polymer endovascular prosthesis and its implantation in porcine arteries. *J. Interv. Cardiol.*, **5** (1992), 175–85.

[VAe] van der Giessen, W.J., Vanbeusekom H.M.M., Vanhouten, C.D., Vanwoerkens, L.J., Verdouw, P.D., and Serruys, P.W., Coronary stenting with, polymer-coated and uncoated self-expanding endoprostheses in pigs. *Coronary Artery Disease*, **3** (1992), 631–40.

[VEa] Vert, M., Li, S., Garreau, H., et al., Complexity of the hydrolytic degradation of aliphatic polyesters. *Angew Makromol Chem.*, **247** (1997), 239–53.

[VEb] Vert, M., Li, S.M., Spenlehauer, G., and Guerin, P., Bioresorbability and biocompatibility of aliphatic polyesters. *J. Mater. Sci. Mater. Med.*, **3** (1992), 432–46.

[VEc] Vert, M., Aliphatic polyesters: Great degradable polymers that cannot do everything. *Biomacromolecules*, **6** (2005), 538–46.

[VIa] Virmani, R., Liistro, F., Stankovic, G., et al., Mechanism of late instent restenosis after implantation of a paclitaxel derivate-eluting polymer stent system in humans. *Circulation*, **106** (2002), 2649–51.

[WEa] Weir, N.A., Buchanan, F.J., Orr, J.F., and Dickson, G.R., Degradation of poly-L-lactide. Part 1: In vitro and in vivo physiological temperature degradation. *Proc Inst Mech Eng [H]*, **218** (2004), 307–19.

[WEb] Weir, N.A., Buchanan, F.J., Orr, J.F., Farrar, D.F., and Dickson, G.R., Degradation of poly-L-lactide: Part 2: Increased temperature accelerated degradation. *Proceedings of the Institution of Mechanical Engineers Part H-J. Eng. Med.*, **218** (2004), 321–30.

[WEc] Wentzel, J.J., Krams, R., Schuurbiers, J.C., et al., Relationship between neointimal thickness and shear stress after Wallstent implantation in human coronary arteries. *Circulation*, **103** (2001), 1740–5.

[WEd] Wentzel, J.J., Whelan, D.M., van der Giessen, W.J., et al., Coronary stent implantation changes 3-D vessel geometry and 3-D shear stress distribution. *J. Biomech.*, **33** (2000), 1287–95.

[WHa] Whelan, D.M., van Beusekom, H.M., and van der Giessen, W.J., Mechanisms of drug loading and release kinetics. *Semin. Interv. Cardiol.*, **3** (1998), 127–31.

[WIa] Williams, D.F., Biodegradation of surgical polymers. *J. Mater. Sci.*, **17** (1982), 1233–46.

[YAa] Yamawaki, T., Shimokawa, H., Kozai, T., et al., Intramural delivery of a specific tyrosine kinase inhibitor with biodegradable stent suppresses the restenotic changes of the coronary artery in pigs in vivo. *J. Am. Coll. Cardiol.*, **32** (1998), 780–6.

[YEa] Ye, Y.W., Landau, C., Willard, J.E., et al., Bioresorbable microporous stents deliver recombinant adenovirus gene transfer vectors to the arterial wall. *Ann. Biomed. Eng.*, **26** (1998), 398–408.

[YOa] Yoon, J.S., Jin, H.J., Chin, I.J., Kim, C., and Kim, M.N., Theoretical prediction of weight loss and molecular weight during random chain scission degradation of polymers. *Polymer*, **38** (1997), 3573–9.

[ZAa] Zahn, R., Hamm, C.W., Schneider, S., et al., Incidence and predictors of target vessel revascularization and clinical event rates of the

sirolimus-eluting coronary stent (results from the prospective multicenter German Cypher Stent Registry). *Am. J. Cardiol.*, **95** (2005), 1302–8.

[ZHa] Zhang, Y., Zale, S., Sawyer, L., and Bernstein, H., Effects of metal salts on poly(DL-lactide-co-glycolide) polymer hydrolysis. *J. Biomed. Mater. Res.*, **34** (1997), 531–8.

[ZIa] Zidar, J., Lincoff, A., and Stack, R., Biodegradable stents. In: Topol, E.J., Ed. **Textbook of Interventional Cardiolology**. 2nd ed. WB Saunders, Philadelphia (1994), 787–802.

[ZIb] Zilberman, M., Nelson, K.D., and Eberhart, R.C., Mechanical properties and in vitro degradation of bioresorbable fibers and expandable fiber-based stents. *J. Biomed. Mater. Res. B Appl. Biomater.*, **74** (2005), 792–9.

[ZIc] Zilberman, M., Schwade, N.D., and Eberhart, R.C., Protein-loaded bioresorbable fibers and expandable stents: Mechanical properties and protein release. *J. Biomed. Mater. Res. B Appl. Biomater.*, **69** (2004), 1–10.